U.S. Department of Transportation

Federal Railroad Administration

Framework for Wheel Life Model – Phase I

Office of Research,
Development,
and Technology
Washington, DC 20590

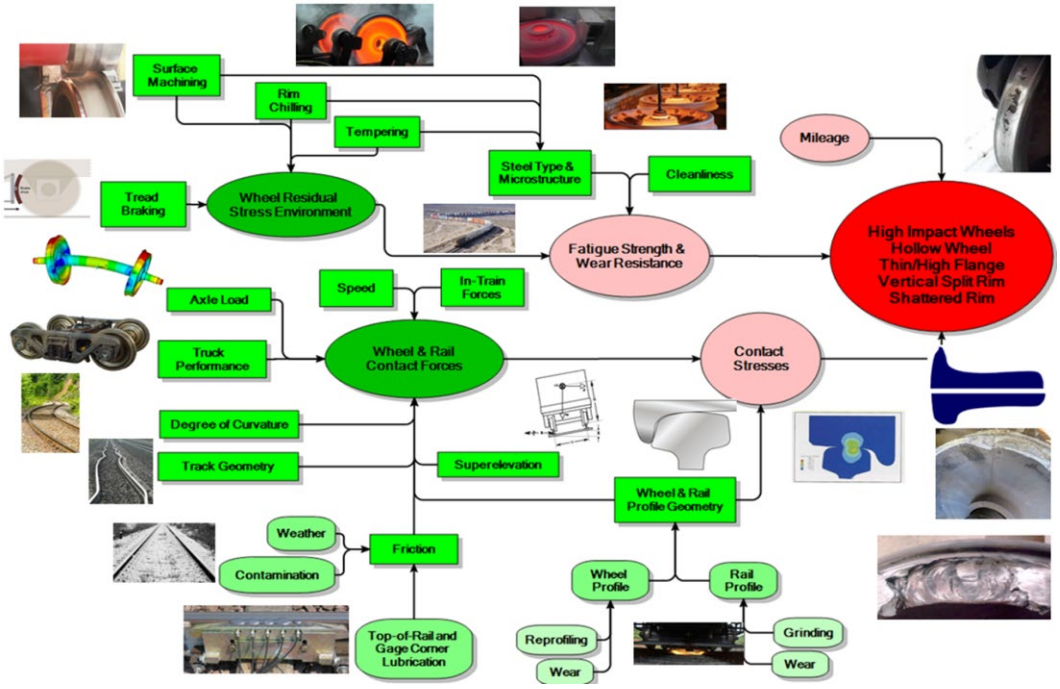

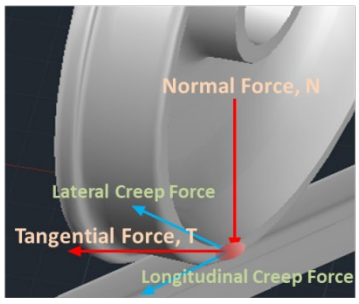

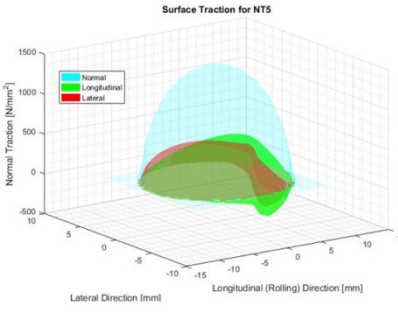

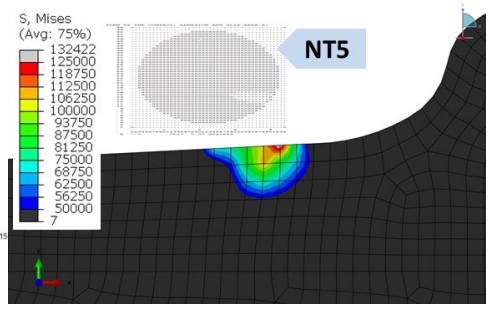

DOT/FRA/ORD-22/25

Final Report
June 2022

REPORT DOCUMENTATION PAGE

Form Approved

OMB No. 0704-0188

1. AGENCY USE ONLY (Leave blank)	2. REPORT DATE	3. REPORT TYPE AND DATES COVERED
	June 2022	Technical Report

4. TITLE AND SUBTITLE
Framework for Wheel Life Model – Phase I

5. FUNDING NUMBERS
693JJ618C000008
FR8RPD32000000008

6. AUTHOR(S)
Bora Jang and Som P. Singh

7. PERFORMING ORGANIZATION NAME(S) AND ADDRESS(ES)
Sharma & Associates, Inc.
100 W. Plainfield Road
Countryside, IL 60525

8. PERFORMING ORGANIZATION REPORT NUMBER

9. SPONSORING/MONITORING AGENCY NAME(S) AND ADDRESS(ES)
U.S. Department of Transportation
Federal Railroad Administration
Office of Railroad Policy and Development
Office of Research, Development, and Technology
Washington, DC 20590

10. SPONSORING/MONITORING AGENCY REPORT NUMBER
DOT/FRA/ORD-22/25

11. SUPPLEMENTARY NOTES
COR: Tarek Omar, Ph.D.

12a. DISTRIBUTION/AVAILABILITY STATEMENT
This document is available to the public through the FRA website.

12b. DISTRIBUTION CODE

13. ABSTRACT (Maximum 200 words)

Researchers developed a model to predict the life of a freight railroad car wheel due to rolling contact fatigue, crack initiation and growth leading to fracture. The Phase I effort includes a literature survey, an estimation of hoop residual stress from manufacturing process, and the effects of mechanical load – including traction and thermal load due to tread-braking on the initial residual stresses distribution in the wheel. An analysis shows how a severe braking event may completely eliminate the beneficial hoop residual stress in the rim of a wheel, which can otherwise delay crack initiation and growth. An approach to include the residual stress in the shakedown theory used to predict rolling contact fatigue is proposed to investigate crack initiation and growth.

14. SUBJECT TERMS
Rolling contact fatigue, contact stress, crack growth, crack initiation, creep, fatigue strength, heat treatment, pearlite, wheel damage map, quenching, residual stress, S-660, shakedown, time-temperature-transformation, tread-braking

15. NUMBER OF PAGES
68

16. PRICE CODE

17. SECURITY CLASSIFICATION OF REPORT	18. SECURITY CLASSIFICATION OF THIS PAGE	19. SECURITY CLASSIFICATION OF ABSTRACT	20. LIMITATION OF ABSTRACT
Unclassified	Unclassified	Unclassified	

METRIC/ENGLISH CONVERSION FACTORS

ENGLISH TO METRIC

LENGTH (APPROXIMATE)

1 inch (in)	=	2.5 centimeters (cm)
1 foot (ft)	=	30 centimeters (cm)
1 yard (yd)	=	0.9 meter (m)
1 mile (mi)	=	1.6 kilometers (km)

AREA (APPROXIMATE)

1 square inch (sq in, in^2)	=	6.5 square centimeters (cm^2)
1 square foot (sq ft, ft^2)	=	0.09 square meter (m^2)
1 square yard (sq yd, yd^2)	=	0.8 square meter (m^2)
1 square mile (sq mi, mi^2)	=	2.6 square kilometers (km^2)
1 acre = 0.4 hectare (he)	=	4,000 square meters (m^2)

MASS - WEIGHT (APPROXIMATE)

1 ounce (oz)	=	28 grams (gm)
1 pound (lb)	=	0.45 kilogram (kg)
1 short ton = 2,000 pounds (lb)	=	0.9 tonne (t)

VOLUME (APPROXIMATE)

1 teaspoon (tsp)	=	5 milliliters (ml)
1 tablespoon (tbsp)	=	15 milliliters (ml)
1 fluid ounce (fl oz)	=	30 milliliters (ml)
1 cup (c)	=	0.24 liter (l)
1 pint (pt)	=	0.47 liter (l)
1 quart (qt)	=	0.96 liter (l)
1 gallon (gal)	=	3.8 liters (l)
1 cubic foot (cu ft, ft^3)	=	0.03 cubic meter (m^3)
1 cubic yard (cu yd, yd^3)	=	0.76 cubic meter (m^3)

TEMPERATURE (EXACT)

[(x-32)(5/9)] °F = y °C

METRIC TO ENGLISH

LENGTH (APPROXIMATE)

1 millimeter (mm)	=	0.04 inch (in)
1 centimeter (cm)	=	0.4 inch (in)
1 meter (m)	=	3.3 feet (ft)
1 meter (m)	=	1.1 yards (yd)
1 kilometer (km)	=	0.6 mile (mi)

AREA (APPROXIMATE)

1 square centimeter (cm^2)	=	0.16 square inch (sq in, in^2)
1 square meter (m^2)	=	1.2 square yards (sq yd, yd^2)
1 square kilometer (km^2)	=	0.4 square mile (sq mi, mi^2)
10,000 square meters (m^2)	=	1 hectare (ha) = 2.5 acres

MASS - WEIGHT (APPROXIMATE)

1 gram (gm)	=	0.036 ounce (oz)
1 kilogram (kg)	=	2.2 pounds (lb)
1 tonne (t)	=	1,000 kilograms (kg)
	=	1.1 short tons

VOLUME (APPROXIMATE)

1 milliliter (ml)	=	0.03 fluid ounce (fl oz)
1 liter (l)	=	2.1 pints (pt)
1 liter (l)	=	1.06 quarts (qt)
1 liter (l)	=	0.26 gallon (gal)
1 cubic meter (m^3)	=	36 cubic feet (cu ft, ft^3)
1 cubic meter (m^3)	=	1.3 cubic yards (cu yd, yd^3)

TEMPERATURE (EXACT)

[(9/5) y + 32] °C = x °F

QUICK INCH - CENTIMETER LENGTH CONVERSION

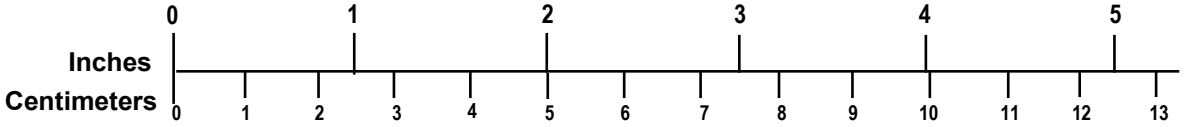

QUICK FAHRENHEIT - CELSIUS TEMPERATURE CONVERSION

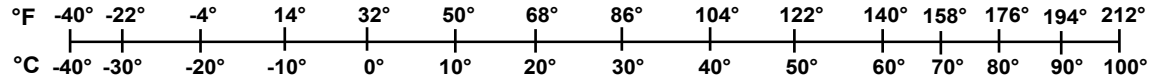

For more exact and or other conversion factors, see NIST Miscellaneous Publication 286, Units of Weights and Measures. Price $2.50 SD Catalog No. C13 10286

Updated 6/17/98

Contents

Illustrations

Tables

Executive Summary

A research team from Sharma & Associates, Inc. is developing an analytical framework to understand the mechanisms limiting the life of freight railroad wheels due to rolling contact fatigue and crack initiation and growth leading to fracture. The research effort comprises two phases: (I) a framework to develop an advanced railway wheel life model for the crack initiation, and (II) expanding Phase I and creating the model to simulate crack propagation under developed wheel operation scenarios. Finally, crack initiation life from Phase I and crack propagation life cycle from Phase II will be combined to develop the baseline for a North American wheel life model.

This report describes Phase I work, which focuses on the literature describing mechanisms and phenomenon affecting wheel life and analytical methods to understand how wheel material properties, manufacturing process, and mechanical and thermal loads in service – along with the operating environment – determine wheel life.

Researchers conducted analytical modeling to estimate the residual stresses induced during quenching and heat treatment, which can delay contact fatigue and crack initiation. They found that residual stresses reduced tread surface and subsurface stresses due to wheel-rail contact loads. Although the thermal load under drag-braking, normal service, and emergency stop conditions introduced significant thermal stresses in the tread and rim areas, the wheel generally remained in an elastic state, i.e., the beneficial residual stresses developed during the manufacturing process did not diminish.

However, severe thermal loading conditions, such as when the hand brakes are left applied, can significantly diminish the beneficial hoop residual stress in the tread and rim and even result in tensile stresses, depending on the duration and magnitude of the applied hand brake force. Such loading early in the life of a wheel would tend to promote premature crack initiation and crack growth on the tread and in the rim.

The team used shakedown theory to predict the conditions for rolling contact fatigue (RCF). Traction loads generated under heavy braking and during curve negotiation result in the accelerated shakedown on the tread surface. When longitudinal traction loads occur due to braking and under curving traction, lateral wheel loads are mostly generated under curving. Thus, a wheel in railroad service, where high degree curves are frequently encountered, would experience significant traction loads. These loads tend to be higher when wheel-rail interface conditions are dry, i.e., with high friction coefficients.

A model to predict RCF crack initiation as a function of wheel load, material strength, traction coefficient, and hoop residual stress on the wheel tread surface is proposed. Although it cannot quantitatively determine the fatigue life of the wheel, it can provide the state of wheel condition indicating potential for RCF crack initiation. Further, the model can be used in a comprehensive approach to estimate wheel fatigue life and allow improvements in the safety and service life of wheels.

Phase II will focus on developing the model to simulate crack propagation by including phenomena such as modeling of metallurgical defects, fluid entrapment, and to estimate crack propagation life under developed wheel operation scenarios.

1. Introduction

This report describes the first phase of a two-phase project to develop a method for calculating railway wheel life given the design, manufacturing process, and operating environment.

1.1 Background

Railway vehicles, using steel wheels rolling on steel rails, constitute the most fuel-efficient transportation system for moving large volumes of goods over long distances. Over time, the tonnage carried per wheel has increased, thus subjecting the wheel-rail contact area to higher and higher stresses. These higher stresses have accelerated the problem of rolling contact fatigue (RCF). From 2000 through 2020, there were 1,051 wheel-related derailments in the U.S. [1], 409 of which were caused by broken wheels (flange, rim, tread, or plate parts of wheel as shown in Figure 1-1). The majority of these 409 derailments were due to a broken rim, such as a shattered or vertical split rim – a manifestation of RCF. Wheel tread shells resulting from RCF and other tread defects such wheel flats result in high wheel impact loads. These loads can range from 2 to 3 times the static wheel load and accelerate wheel failures that annually cost North American freight railroads $400 million [2].

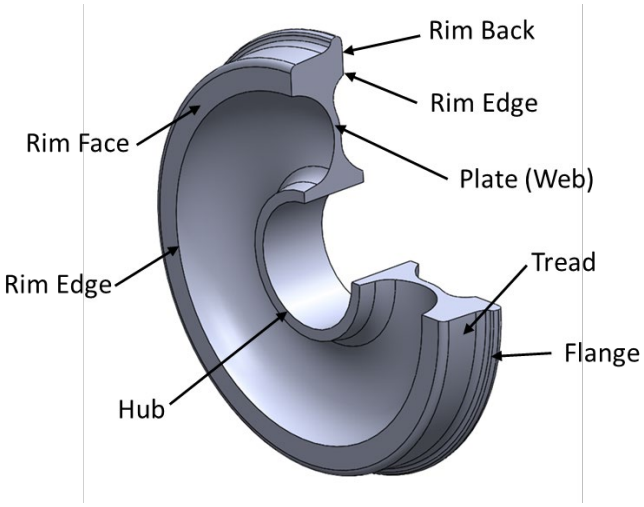

Figure 1-1. Anatomy of a railway wheel

Wheel life has improved over the years, despite increased axle loads, owing to RCF research programs supported by the Federal Railroad Administration (FRA) and the Association of American Railroads (AAR). However, the consequences of RCF still remain the significant cause of wheel-related derailments and one of the major rolling stock maintenance cost in North America. Therefore, there is a need for a comprehensive analytical methodology to understand and quantify the mechanics and root causes of RCF within the context of North American heavy-haul practices.

Organizations such as International Heavy Haul Association have published best practices [3] to reduce RCF in heavy-haul service; the recommendations have been primarily based on test studies and wheel and rail maintenance practices. An analytical model supported by test results would provide capabilities to evaluate design and service condition changes to develop improved maintenance plans and practices to minimize wheel failure.

Several practices can extend wheel life, including the introduction of high-performance wheels, steering trucks, top-of-rail lubrication units for friction management at curves, track geometry improvements, and superelevation optimization. However, the estimation of the benefits resulting from these improvements is not straightforward. A wheel life model envisioned and pursued in this research effort can provide the critical quantitative information to design safer and more efficient operating and maintenance strategies.

1.2 Objectives

The overall objective of this research is to develop a framework and analytical model for estimating life of wheels in North American freight rail service. The objective of Phase I is to conceptually develop a railway wheel life model and investigate factors leading to RCF and crack initiation. Identifying the forces and contact environment that delays crack initiation can lead to developing guidelines for optimum wheel and rail interface management procedures and safety improvements.

1.3 Overall Approach

The approach for Phase I was to review the published works in the field of wheel RCF, wear, and crack propagation. The literature search and review allowed researchers to develop a methodology to estimate manufacturing residual stresses, contact stress under mechanical and thermal loads and their combination. Finite element analysis (FEA) software was used to investigate the load conditions that result in stress-state controlling crack initiation and growth potential due to the wheel tread surface and sub-surface RCF.

1.4 Scope

The scope of this research project includes wheels in freight interchange service in North America. The wheels are subject to tread-braking. Their material properties conform to the relevant Association of American Railroads standards.

A typical wheel is used to demonstrate the analytical methods described in this report. The wheel is Class C with 36-inch diameter.

1.5 Organization of the Report

This report is divided into the following sections:

Section 2 summarizes the relevant literature, including published academic papers, institutional and industry research reports, and conference proceedings.

Section 3 discusses the wheel manufacturing process, including the heat treatment used to impart compressive residual stresses to the tread and rim area. It describes an analytical approach to estimate these stresses.

Section 4 shows the effect of wheel-rail contact forces on the compressive hoop residual stresses in the wheel.

Section 5 includes analysis of wheel thermal loading due to tread-braking and its effects on the compressive hoop residual stresses in the wheel.

Section 6 describes the combined effects of wheel-rail contact forces and tread-braking on the compressive hoop residual stresses in the wheel.

Section 7 discusses shakedown theory and a proposed RCF crack initiation model.

Section 8 gives a conclusion for Phase I and outlines the work planned for Phase II.

2. Literature Review

Wheel performance is controlled and affected by a myriad of factors, as shown in Figure 2-1. Based on the wheel metallurgy and operating conditions [4] such as truck steering characteristics, wheel and rail interface coefficient of friction (lubrication practices, contamination, weather, etc.), track geometry, axle load, speed, route (number and sharpness of curves, grades, loaded traffic direction, etc.), train handling, brake applications, and track grinding and profiling practices, the wheel failure mechanism and life can change significantly.

There are specifications for wheel design load, geometry, and properties of the wheel steel material. Wheels are replaced in service for various reasons, the major ones being wear, fatigue, and fracture, with well-defined sub-causes as follows:

- Wear: Thin rim, thin flange, high flange, vertical flange, and tread hollow
- Fatigue and fracture: Thermal cracks, rim cracked, rim shattered, and tread shelled

Besides these well-defined phenomena and associated measurable parameters, there are 18 other causes defined in the Association of American Railroads (AAR) Field Manual [5] for which a wheel should be taken out of service and replaced, confirming the difficulty of establishing a universal definition of wheel life. However, the most significant factors affecting the in-service performance of wheels are as follows:

- Residual stress state from manufacturing
- Material properties
- Wheel and rail profiles
- Wheel-rail contact forces
- Operating environment including speed and braking

There is a significant volume of published material on wheel RCF and wear. A thorough literature search revealed over 330 articles published in various journals, presented at international and domestic conferences and in-house research reports, were gathered for this literature survey. These research articles were sorted into six major categories corresponding to the most significant factors listed above. Further sorting of these items has been conducted where a study or investigation was found to cover more than one category. Also, these articles have been ranked in chronological order to provide a guide as to how the state of research has evolved and progressed with advances in material properties characterization, failure mode models, and more computationally-efficient analytical software.

This literature compilation helped in understanding the various modeling techniques used in wheel life modeling research and to refine the framework for studying wheel failure mechanisms.

This report focuses on determining (1) the residual stress state in wheels from the effects of manufacturing and service conditions, (2) wheel-rail contact stresses, and (3) crack initiation phenomenon induced by RCF. The following sub-sections discuss the published works in these areas.

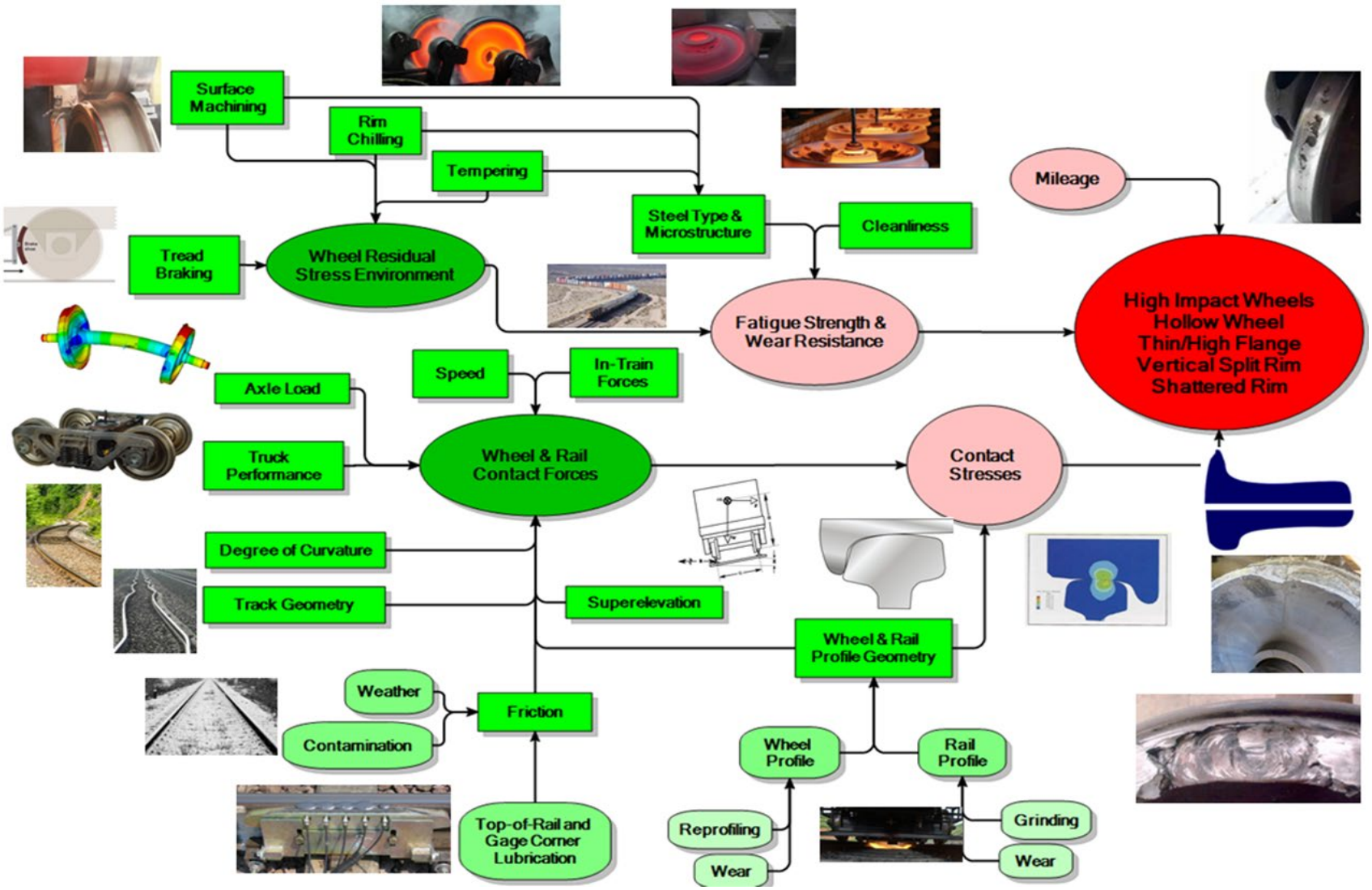

Figure 2-1. Wheel life flowchart

2.1 Residual Stresses in the Wheel

Residual stresses exist in the body of a structure after removing applied loads. For wheels, these stresses can develop during the manufacturing process and can be controlled to create a stress state that improves wheel performance.

The initial residual stress can be modified after exposure to service conditions and mechanical and thermal loads if the loading conditions result in non-elastic stresses due to overload or a change in material properties such as elevated temperature.

In general, compressive residual stresses help prevent the formation and growth of cracks in the wheel tread and rim area. Since the residual stresses are not visible and difficult to measure, a theoretical method is useful to estimate them.

Kuhlman et al. [6] described an analytical model to estimate stresses during the quenching and tempering of a railroad wheel. In the study, the effects of time-dependent deformation and temperature-dependent properties on the residual stress were determined. The paper includes the change in characteristics such as the specific heat and thermal conductivity during material phase transformation as the temperature of wheel changed. Further, the paper emphasizes that time-dependent creep significantly affects the circumferential (hoop), axial, and radial residual stresses.

Gordon et al. [7] conducted a detailed study of the estimation of residual stresses in railroad commuter car wheels during the manufacturing process with consideration for the time-dependent creep effect introduced by Kuhlman et al [6]. The effect of carbon content on the changes in microstructure during transformation was analyzed in detail.

Wang et al. [8] conducted FEA for the heat treatment process of a 36-inches (91.44-cm) Class C freight wheel. This study evaluated the effects of ideal and non-ideal heat treatment on the residual stress distribution in a wheel with the time-dependent thermal and mechanical material properties.

In addition, Wang et al.[8] investigated the effect of thermal load due to tread-braking on the residual stress level on the tread surface, and included the initial residual stress in the wheel. In this analysis, the heat treated material properties were considered. They observed that the hoop residual stress in the wheel tread and rim can change from compression to tension under severe braking.

Gordon et al. [9] also investigated the effects of service conditions on the residual stress distribution in commuter car wheels with initial residual stress from the manufacturing process. The analytical work considered contact loads due to wheel and rail interaction and thermal loads from tread-braking. The results indicated that the initial compressive hoop residual stress was reversed to tension. It showed that the predicted depth of tensile residual stress agreed well with the depth of thermal cracking observed on the wheel.

2.2 Wheel and Rail Contact Stresses

RCF causes premature wheel and rail failures. Repeated application of excessive contact pressure and shear stresses under traction loads on the wheel and rail surfaces leads to RCF, which is a combination of multiaxial fatigue and wear mechanisms.

Safety risks associated with RCF in North American freight railways can be mitigated by implementing the appropriate wheel and rail interface management strategies and operational practices. With the trend of increasing axle loads, RCF is likely to remain as a major source of safety risk. Thus, there has been significant research into rolling contact mechanics since the pioneering works of Kalker [10] and Johnson [11].

The program CONTACT [12] uses the rolling contact mechanics theories of Kalker. It can solve three-dimensional frictional rolling contact problems to determine the stress-strain environment in the wheel and rail contact zone [13].

Then, Kalker [14] developed the Future Automotive Systems Technology Simulator (FASTSim) tool for a simplified theory of rolling contact. A second version of FASTSim was developed by Vollebregt et al. [15] to obtain more accurate results of contact forces. It is the standard tool for multibody vehicle dynamics wheel and rail force simulations to determine the wheel-rail contact creep force.

Lundén [16] and Gordon et al. [9] used FEA to determine the shakedown residual stress states on wheels for the combined effect of contact forces and braking. Temperature-dependent material data for a wheel steel were used for both studies. Hertz theory was used for the contact model of the wheel and rail contact interference. However, while Gordon et al. [9] considered the existing initial residual stresses induced by the heat treatment process, Lundén [16] assumed the wheel had no residual stresses. In both analyses, the axisymmetric geometry and loading were assumed, to reduce modeling complexity and computational time.

2.3 Rolling Contact Fatigue Crack Initiation

Wheel (rim and tread) damage can occur due to both fatigue and wear failure mechanisms. For railway vehicle wheels, repeated high stresses accelerate RCF. Wang et al.[8], Gordon et al. [9], Kabo et al. [17], and Ekberg et al. [18] indicated a reduction in protective residual stresses under tread-braking and the presence of metallurgical defects (non-metallic inclusions and voids) promote subsurface and surface crack initiation and propagation.

The propagation of surface-initiated cracks can be exacerbated by the ingress of water, ice, grease, and other contaminants. Crack-tip pressurization and crack surface friction reduction, due to an entrapped substance, are expected to accelerate crack propagation [18, 19].

Another scenario is subsurface crack formation and propagation. Ekberg et al. [18] investigated that a subsurface crack tip frequently turns toward the surface, and shelling occurs. Another possibility is the merging of subsurface and surface-initiated cracks near the tapeline zone of the wheel tread. Infrequently, a subsurface crack tip turns toward the hub and results in a broken wheel rim.

RCF initiation can be predicted using shakedown theory [11, 20, 21, 22, 23, 24]. In metal plasticity theory, elastic shakedown is a stress limit above a material's yield strength where the material behaves elastically with some residual stresses developed under initial yield.

Johnson and his co-researchers [20, 21, 22, 23, 24] applied this plasticity phenomenon to rolling continuum mechanics and determined a shakedown limit, as shown in Figure 2-2. The x-axis of the shakedown diagram is a traction coefficient, which is the ratio between tangential and normal force. It can be interpreted as the demand for adhesion. This value is bound by the available

friction coefficient. The y-axis is the ratio between maximum contact pressure and the shear yield strength of the material.

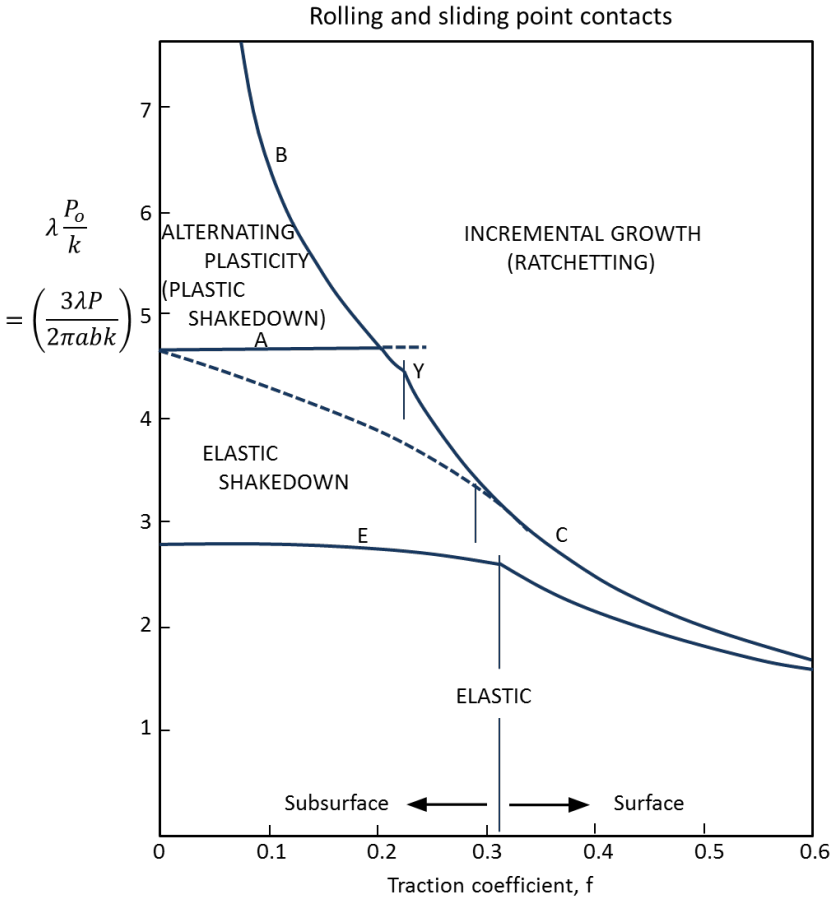

Figure 2-2. Shakedown diagram for point contact [21]

As long as the contact conditions remain below the elastic shakedown limit, maximum fatigue life (theoretical infinite life) is expected. If contact conditions exceed the elastic shakedown limit then surface or subsurface RCF can be expected. Sabri et al. [4] used shakedown theory to predict RCF initiation for a 36-inch wheel under cyclic normal and traction loads. The load datasets were collected from two revenue service tests on a car equipped with non-steering trucks and steering truck, respectively.

However, this approach has limitations due to assumptions used for several factors, such as contact geometry changes during service, the reduction in residual stresses from the manufacturing process, and the effects of extreme tread-braking events [6, 7, 8, 9].

3. Estimation of Residual Stress: Manufacturing Process

Compressive hoop residual stresses in wheel treads delay crack initiation and propagation. During manufacturing of wheel, whether forged or cast, heat treatment through rim quenching followed by whole wheel annealing is used to develop such stresses in the wheel rim and at the tread surface.

This section describes simulations of heat treatment during the wheel manufacturing process to determine the residual stress distribution in a wheel using an FEA tool for thermal and stress analyses.

3.1 Manufacturing Process Model

For heat treatment, a two-step approach is applied for estimating the residual stresses resulting from the quenching process:

(1) A heat transfer analysis in which the transient temperature distributions as a function of time during the heat treatment process are estimated.

(2) A stress analysis which uses these temperature distributions to estimate the development of the residual stresses after the heat treatment process.

The predicted residual stresses due to the heat treatment are basically the results of the heat transfer and stress analyses. The residual stresses are affected by metallurgical aspects of the process in which the microstructure of a material is transformed depending on temperature to change the mechanical properties.

3.1.1 Wheel Manufacturing Process

Wheels are manufactured using a multi-step process to form the final shape either through the casting or forging process. At the end of either process, the wheel is transferred into a furnace and is uniformly reheated to a high temperature of around 1500 °F (816 °C) to remove undesired residual stresses.

Then the tread of the wheel is quenched by a water spray. The duration of quenching depends on the rim thickness and the wheel diameter. Following quenching, the wheel is placed in a furnace for several hours to reduce the levels of residual stress, a process known as annealing. After annealing, the wheel is left under ambient conditions to cool down to room temperature.

When the tread surface of wheel rim is quenched by the water spray, the outer part of wheel rim is cooled and shrinks. However, the inner parts of rim, plate, and hub are still hot and have the lower yield strength due to the high temperature. After quenching, the wheel is tempered in a furnace to reduce brittleness and to increase toughness. Then the wheels are allowed to cool to room temperature for several hours. This heat treatment results in:

(1) Increased strength of the steel

(2) Improved wear resistance

(3) Desirable compressive hoop residual stress in the wheel rim

In general, the heat treatment process is considered to create or control the magnitude of residual stresses in a target component material [7, 8, 25, 26]. For a wheel, the heat treatment is used to develop compressive residual stresses in the rim and tread. These residual stresses prevent or delay the formation of fatigue cracks and also slow down the growth of these cracks. Thus, the residual stresses in the as-manufactured condition of wheels must be accounted for when assessing the performance of wheels in service.

3.1.2 Candidate Wheel Design for Analyses

The gross rail load for a majority of the current North American freight car fleet is 286,000 lbs (1,272 kN). In this study, a 36-inch (91.44-cm) freight wheel with a wide-flange single-wear rim 1.5-inch (38-mm) thick and parabolic plate for 286,000-lb (1,272-kN) gross rail load (GRL) service was considered.

The vertical static wheel load for a conventional car is 35,750 lbs (159 kN) in the 286,000-lb (1,272-kN) GRL service. The cross-section of the selected wheel is shown in Figure 3-1. According to the Association of American Railroads (AAR) [27], for freight cars in interchange service, Class B, C, or D wheels must be used. Furthermore, all freight car wheels manufactured for AAR interchange service must be heat-treated.

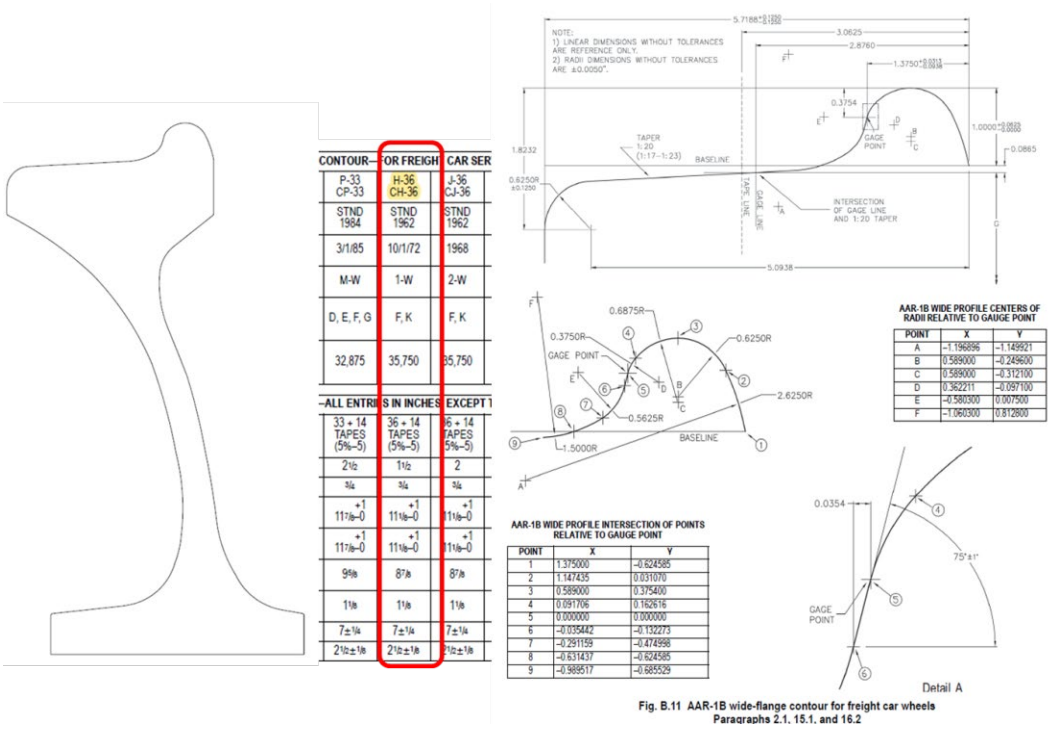

Figure 3-1. Schematic of wheel selection and cross section of 36" wheel [27]

The wheel used in this study was Class C. The required chemical composition of the Class C wheel steel is shown in Table 3-1. The required hardness and the yield strength of a Class C wheel are shown in Table 3-2.

In this study, the following modeling and analyses for heat treatment and in-service conditions were carried out on this most representative wheel.

Table 3-1. Chemical requirements for Class C wheel steel [27]

Element	Carbon, C	Manganese, Mn	Phosphorous, P	Sulfur, S	Silicon, Si
Ladle Analysis (%)	0.67–0.77	0.60–0.90	0.03 max	0.005–0.04	0.15–1.0

Table 3-2. Class C in AAR wheel classes [27]

AAR wheel class	Yield Strength, MPa (ksi)	Hardness, BHN (HRC) MIN-MAX
Class C	620 (90) for Rim	321–363 (35–39)
	380 (55) for Plate	

3.2 Metallurgical Considerations

A time-temperature-transformation (TTT) diagram is used to describe the changes in metallurgy that occur during cooling. Temperature is plotted on the vertical axis, and time is plotted on a logarithmic scale along the horizontal axis in the TTT diagram.

The carbon content for a Class C wheel is between 0.67 and 0.77 percent. The closest steel for such carbon content is eutectoid steel, which is 0.77 percent carbon. The TTT diagram for this steel is presented in Figure 3-2 [28].

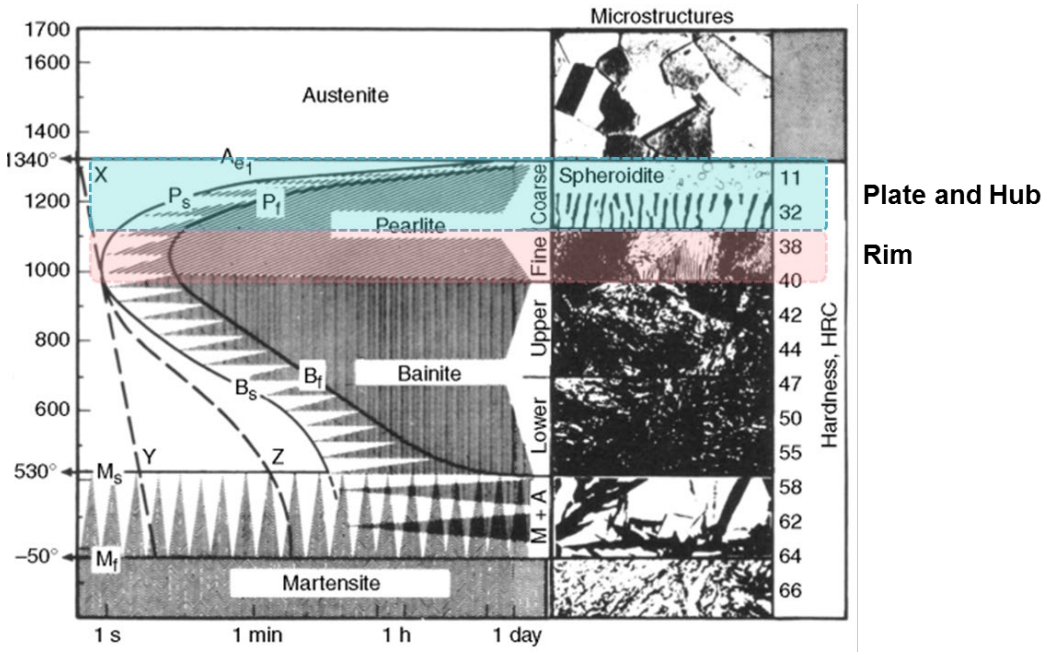

Figure 3-2. TTT diagram for a 0.77 percent (eutectoid) carbon steel [28]

For this material, austenite exists above 1340 °F (725 °C). Transformation begins when the steel is cooled below the temperature for austenite. The resulting microstructure depends on the rate of cooling. It also varies depending on the level of carbon content in the steel. If the steel is rapidly

cooled (e.g., within 1 second), the material will transform into martensite. Martensite is very hard and brittle and thus not suitable as a wheel material.

If the steel is slowly cooled (e.g., within 1 minute), two different phases, ferrite and cementite, are formed – called a eutectoid transformation, in which a phase transforms into two different phases. This transformation produces coarse pearlite. If the steel is cooled and controlled, where the transformation begins in approximately 1 second and is completely transformed in a few minutes, the transformed product becomes fine pearlite.

Pearlite is the desired microstructure for railroad wheel, with fine pearlite in the rim and coarse pearlite in the plate and hub. Quenching in the manufacturing process accelerates cooling and enables pearlite to form when the tread surface of wheel rim is exposed to a water spray for several minutes.

3.3 Finite Element Analysis

Finite element (FE) simulation is performed to determine the residual stress in the wheel due to the heat treatment in the manufacturing process (e.g., quenching, annealing, cool down). The simulation allows the development of thermal and stress time histories as well as the steady-state, final residual stress distribution.

3.3.1 Finite Element Model Description

The simulation is a transient thermal analysis followed by a stress analysis. A three-dimensional model of the wheel was developed with element density varying through the wheel cross-section, with highest density in the tread region, as shown in Figure 3-3. The mesh contained 777,000 nodes and 706,800 hexahedral and wedge elements, as shown in Figure 3-3.

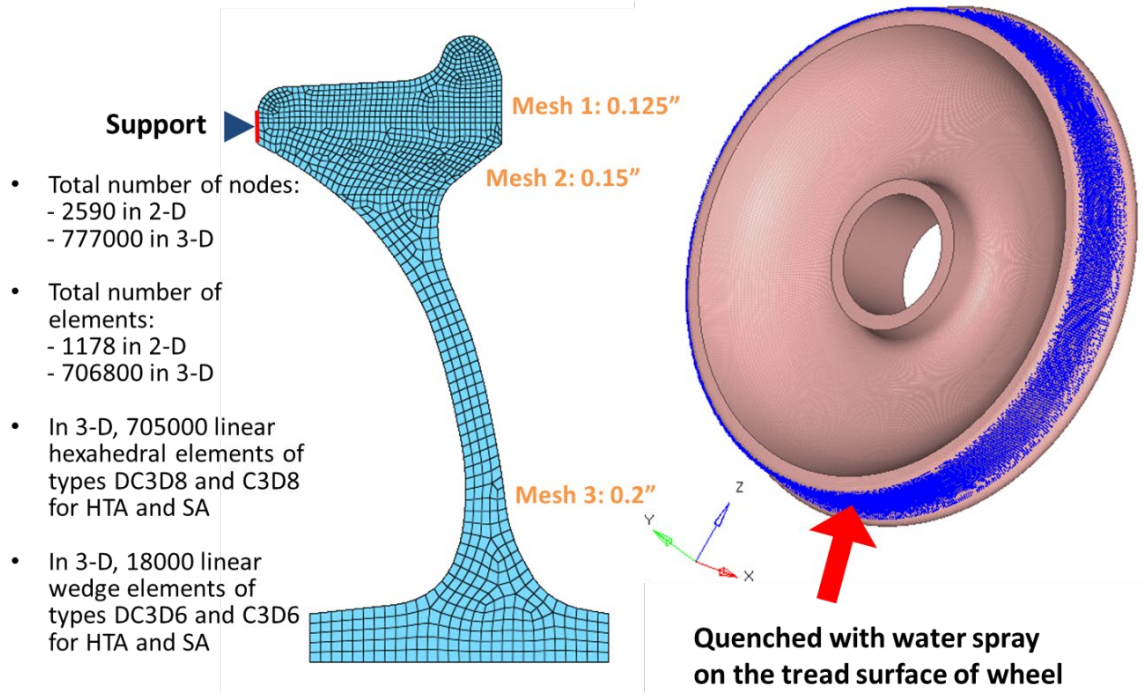

Figure 3-3. FE mesh and water sprayed area for quenching simulation

Transient heat transfer analysis (HTA) was conducted first to obtain the temperature distribution history. Then the temperature distributions were used as an input (i.e., loads) for the stress analysis (SA). Abaqus/Standard, a commercial FEA program [29, 30], was used for the heat transfer and stress analyses.

3.3.2 Heat Transfer Analysis

The initial condition of the wheel in the transient heat transfer analysis was specified as a uniform temperature representing the condition of wheel just removed from the austenitizing furnace. A convection heat transfer load corresponding to the water spray quench was applied to the tread surface, as shown in Figure 3-4 (the same as region in blue in the 3D model in Figure 3-3). Nodal temperatures throughout the model were obtained during the heat transfer portion of the analysis and used for the stress analysis.

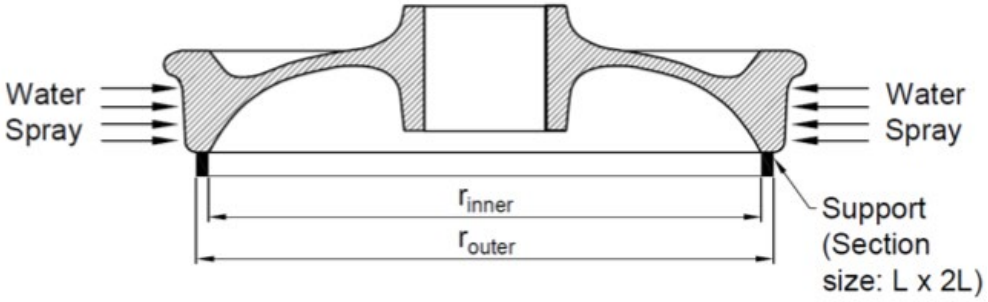

Figure 3-4. Wheel quench schematic with support

The thermal loads were applied in five sequential steps, representing heat treatment process:

Step 1: The pre-quench, representing the environment from the austenitizing furnace to the place for quenching

Step 2: The initial quench from high temperature

Step 3: The dwell at room temperature

Step 4: The elevated temperature annealing

Step 5: The period during which the wheel cools to room temperature.

The steps are schematically presented in Figure 3-5. The quench schedule for heat treatment in Figure 3-5 was selected based on the simulation with variations in annealing and cooling duration; this will be discussed in the following section.

The heat transfer analysis requires the specification of material properties which are dependent on temperature. The parameters for the heat transfer analysis include the thermal conductivity and specific heat, as shown in Figure 3-6 [6, 7, 8, 27, 31].

The heat transfer coefficient (HTC) between the wheel and its surroundings corresponding to convection heat transfer values for freight wheels were obtained from laboratory measurements [6]. During the rest of the process, except the quench, the heat transfer coefficient had a constant value of 5.0 Btu/hr-ft^2-°F (28 W/m^2) on all exposed wheel surfaces.

During the quench, the heat transfer coefficient at the tread was tested with three values: (1) HTC1 is a value of 540 Btu/hr-ft^2-°F (3066 W/m^2) as a constant; (2) HTC2 and (3) HTC3 are

temperature dependent, *f1* and *f2*, respectively, as shown in Figure 3-7 [7, 32, 33]. A value of 5.0 Btu/hr-ft^2-°F (28 W/m^2) is used everywhere except the tread surface.

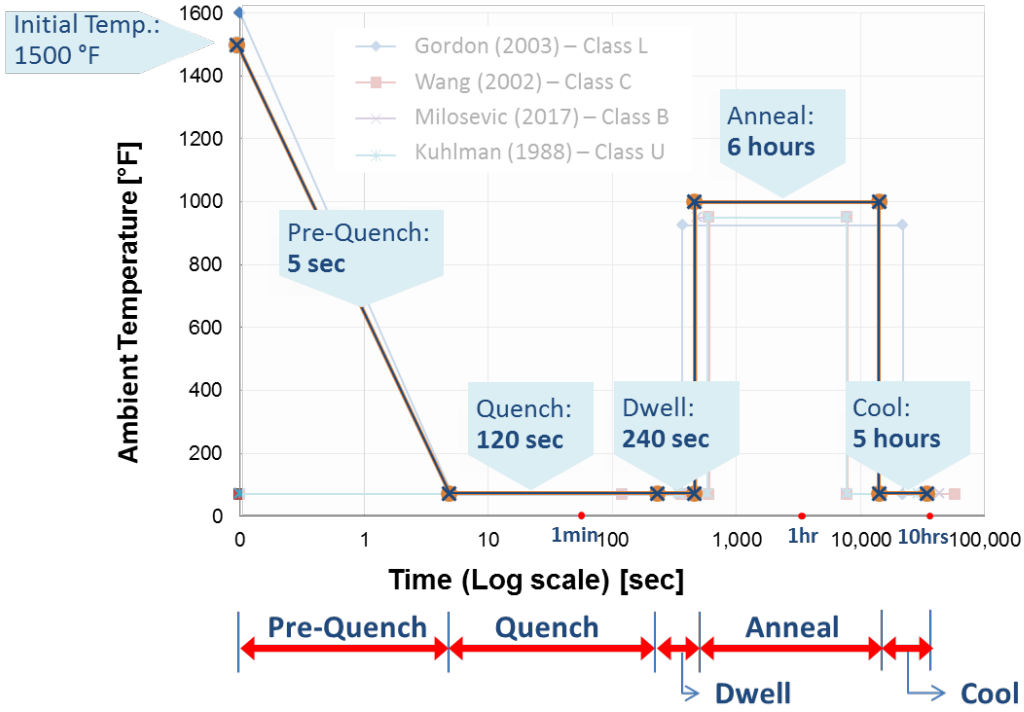

Figure 3-5. Wheel quenching process: ambient temperature vs. time [6, 7, 8, 31]

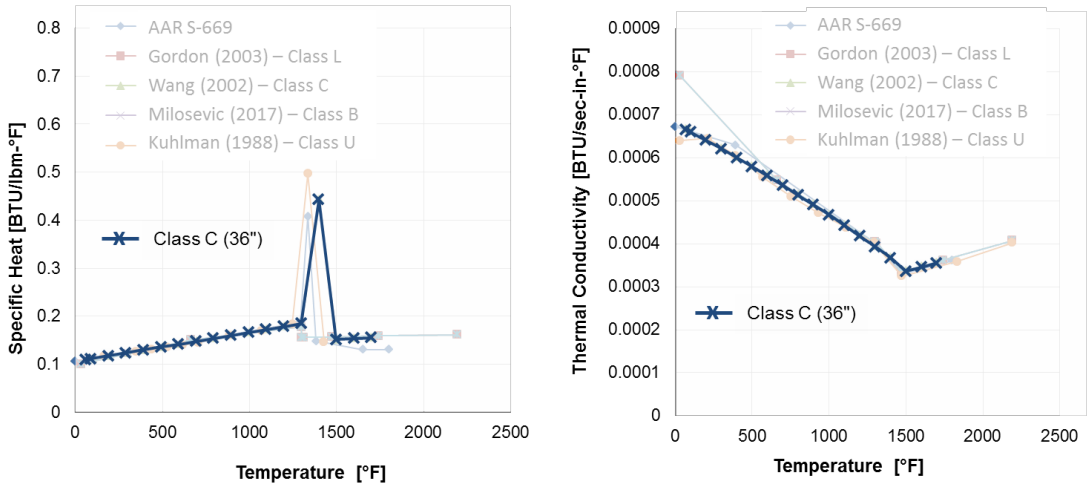

Figure 3-6. Material properties for heat transfer analysis: (a) specific heat and (b) thermal conductivity [6, 7, 8, 27, 31]

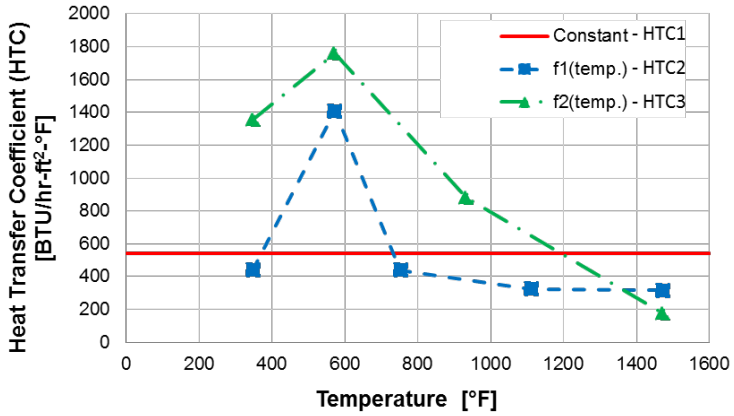

Figure 3-7. Heat transfer coefficient of water spray quench [7, 32, 33]

Radiation heat transfer from the wheel surface is accounted in the heat transfer analysis. The Stefan-Boltzmann constant is 1.71E-13 BTU/hr-ft^2-R^4 (5.67E-08 W/m^2-K^4). Constant radiation surface emissivity, e = 0.95, is assumed for all surfaces [7]. Surface emissivity, e = 0.95, means that the surface radiates well.

3.3.3 Stress Analysis

Stress analysis, to estimate the residual stresses resulting from the heat treatment, followed the heat transfer analysis. This was performed in the same sequential steps as the heat transfer analysis. The FE mesh used in the thermal analysis was also used for the stress analysis.

Previous researchers [6, 7, 8] have determined that creep is an important consideration in such simulations. Thus, the effect of creep has been considered in this study as a significant variable. Viscoelastic creep can be used to represent a stress relaxation phenomenon. Stress relaxation occurs in a stressed body held at an elevated temperature for an extended period. The phenomenon occurs during the annealing phase of the heat treatment process. It was accounted for in the modeling effort through the specification of creep strain rates which are dependent on the local values of temperature and stress. The creep strain rate was estimated by using the equation as follows [6]:

$$\dot{\varepsilon} = 4.64 \times 10^{-08} \left(\sigma_{eff}{}^{12.5}\right) e^{\frac{-53712}{T+460}} \qquad (3.1)$$

Where,

T is the temperature in Fahrenheit, and

σ_{eff} is the von Mises effective stress in ksi (1ksi = 6.895 MPa).

This equation was developed from experimental data and calibrated with appropriate methods to ensure consistent engineering units [6]. The estimated creep strains were obtained from the calculated strain rates. A creep response modeling feature is available in Abaqus and was implemented via a user subroutine [30].

The transient temperature distribution determined during the heat transfer analysis was used as the time-dependent loading for the mechanical stress analysis. Material properties specified in stress analysis are shown in Figure 3-8 [8].

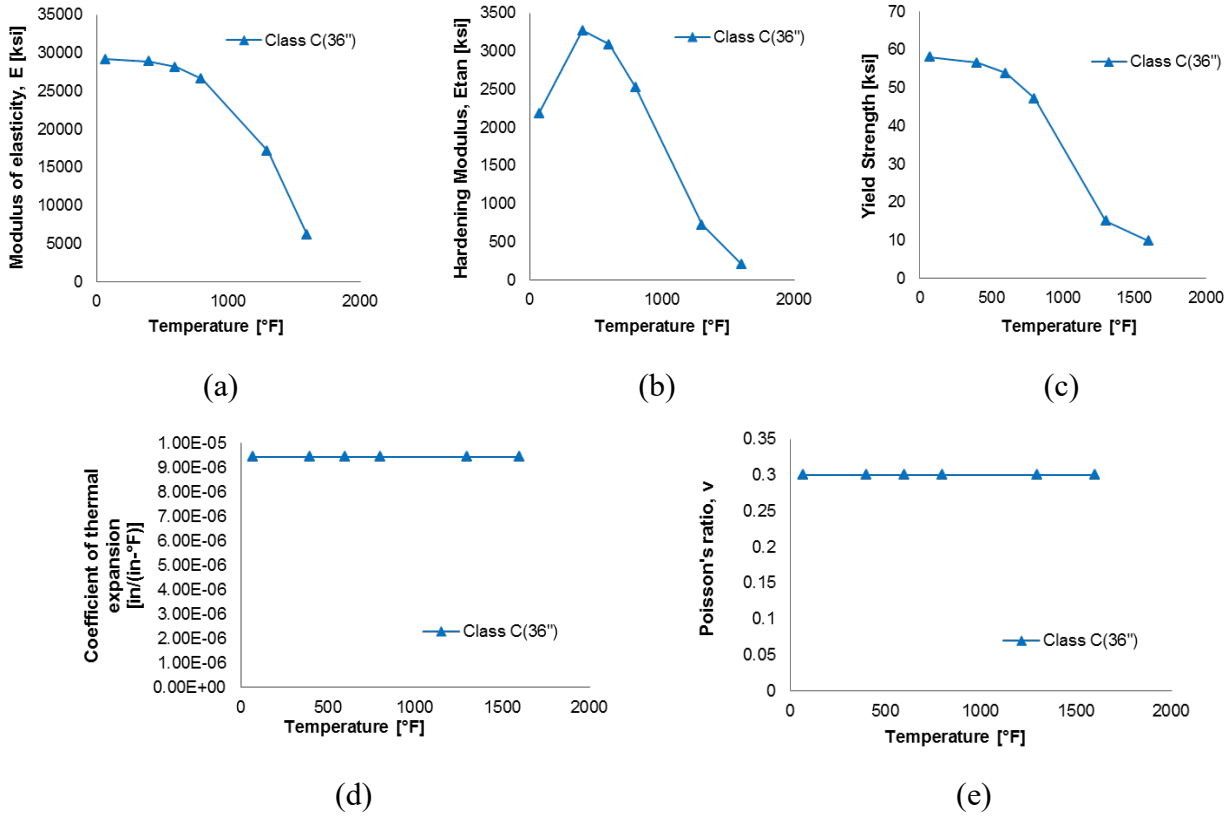

Figure 3-8. Material properties for stress analysis: (a) modulus of elasticity, (b) hardening modulus, (c) yield strength, (d) coefficient of thermal expansion, and (e) Poisson's ratio [8]

3.4 Residual Stress Estimation from Manufacturing Process

This section presents the results of the FEA for the heat treatment from the manufacturing process.

3.4.1 Heat Transfer Analysis

Two variables were considered for the quenching simulation of freight wheels:

(1) Annealing and cooling durations

(2) HTCs

The heat transfer analysis was conducted for four different quench schedules and three different values of heat transfer coefficient during the quenching.

In terms of the quench schedule, different durations of annealing and cooling were examined to determine the baseline condition for the quenching simulation. The case of 6 hours of annealing and 5 hours of cooling was selected based on (1) the temperature at the end of annealing and

cooling and (2) the accuracy of the FEA. The selected quenching schedule is presented in Figure 3-5. The temperature-time history and temperature contour plot at the end of each step for the selected quenching simulation are presented in Figure 3-9. At the end of the quenching step, the temperature was 451 °F (233 °C) on the tread surface and 1430 °F (777 °C) in the rim base.

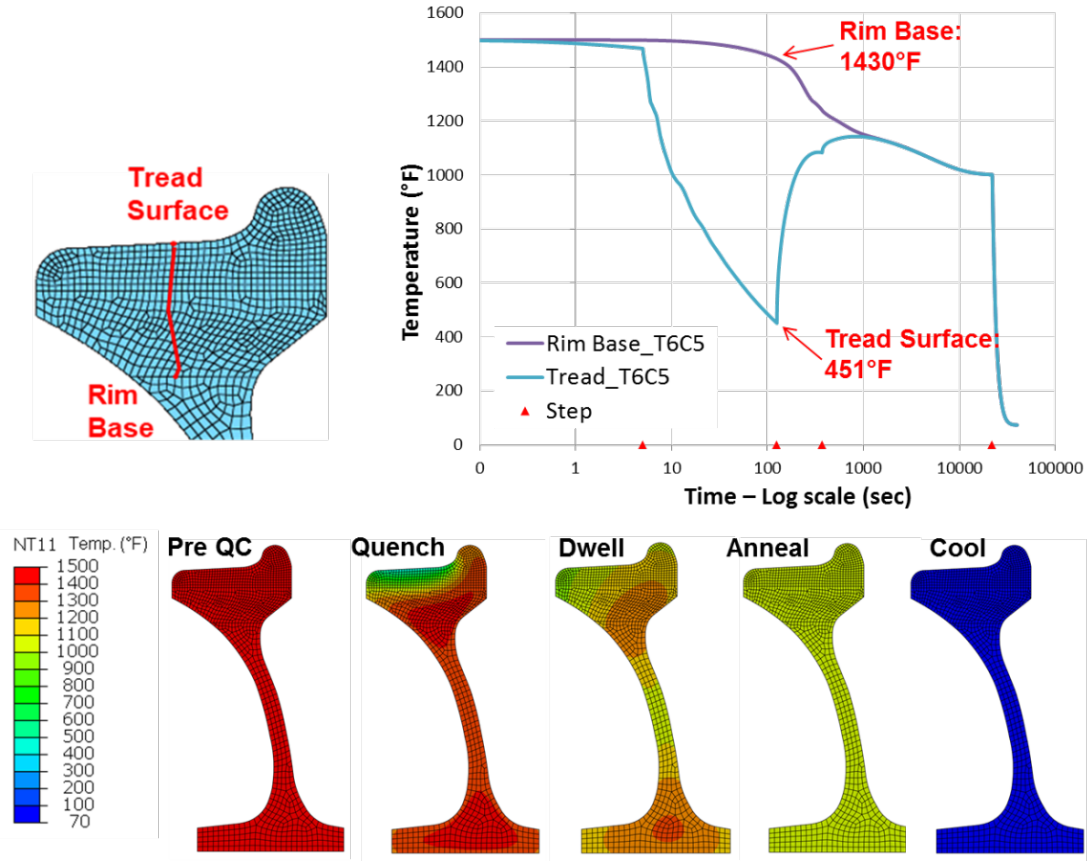

Figure 3-9. Temperature-time histories and contour plot in the wheel section at the end of each step

Figure 3-10 shows the temperature-time histories at the tread surface and the rim base on the TTT diagram for the three simulated values of heat transfer coefficient.

The microstructure in the rim and tread of wheel can be inferred from Figure 3-10. During a water spray quench, all cases of HTC were properly controlled, beginning and completing the transformation from austenite to pearlite for the tread and rim of the wheel. After quenching and dwelling, the temperature of the entire wheel was elevated to annealing temperature, 1000 °F (538 °C), within the duration of annealing for all cases.

To obtain the desired microstructure, which is fine pearlite for the tread of wheel, and the desired level hardness, cases HTC1 and HTC3 during quenching were presented as suitable passes on the TTT curve. However, approximations were made in the relation between the TTT curve and the result in temperature-time shown in Figure 3-10. In addition, all three cases resulted in transforming to coarse pearlite in the rim of the wheel. Therefore, any of three values of HTC may be used as a reasonable parameter in the wheel quench process.

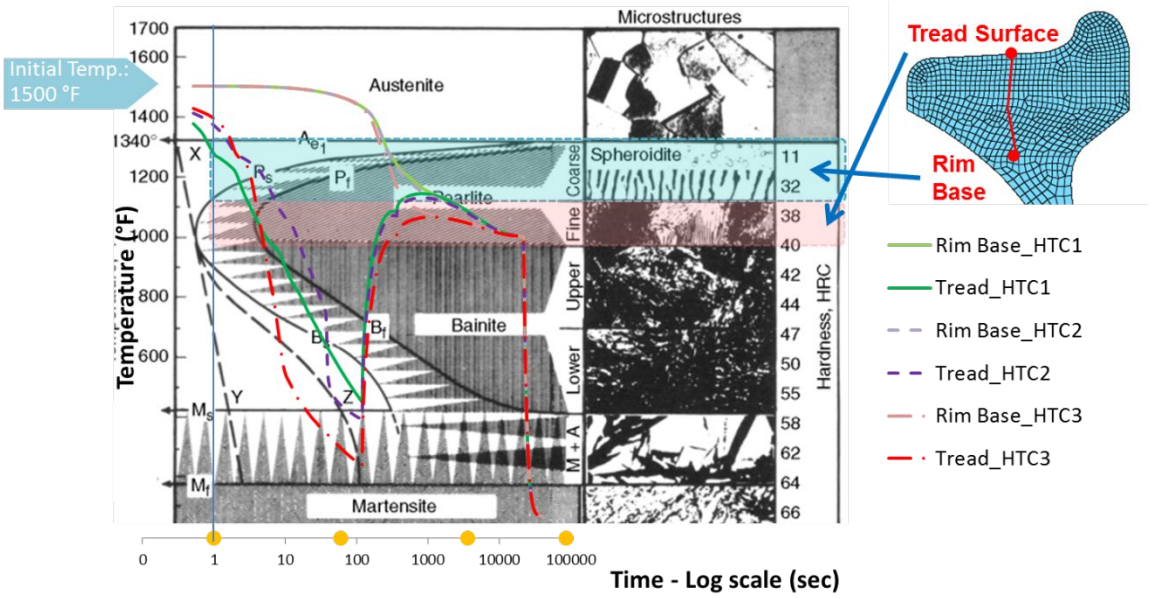

Figure 3-10. Temperature-time history on the TTT diagram with consideration for three values of HTC

3.4.2 Stress Analysis

The stress analysis was conducted using the temperature distribution from the heat transfer analysis to determine the residual stress due to the manufacturing process. As discovered in the previous work on simulation of stress analysis for the heat treatment process [6, 7, 8], creep is most important feature in the simulation. The creep effect is required to accurately predict the as-manufactured residual stress distribution in wheels. In this study, a quenching process simulation for creep effect with HCT1 (constant value) was also conducted; creep made the most important difference during annealing, as shown in Figure 3-11 and 3-12.

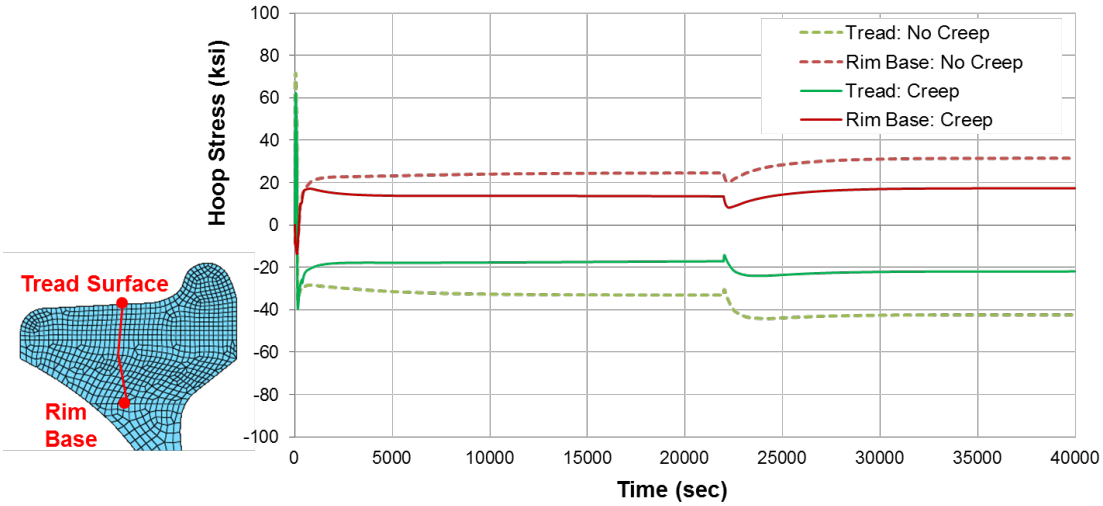

Figure 3-11. Time history of hoop stress during entire quenching process: creep vs. no creep

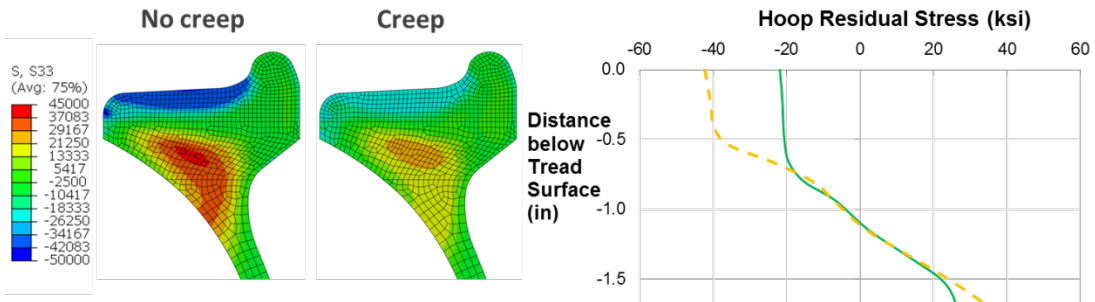

Location	Rim Base	Tread
No Creep	31.5 ksi	-42.3 ksi
Creep	17.3 ksi	-21.9 ksi
Crp./No Crp.	**0.55**	**0.52**

Figure 3-12. Hoop residual stress distribution in the section of wheel rim at the end of process (cooling): creep vs. no creep

It resulted in ~47 percent reduction in the residual stresses at the end of entire quenching process. Thus, the subsequent simulations included the effect of creep through a user subroutine in Abaqus.

The results of the stress analysis, including the effect of creep and different HTCs during the quenching, are presented in Figure 3-13, 3-14, 3-15, and 3-16. The major differences appear in Figure 3-13 and Figure 3-15, which represent the hoop stress at the end of the quench and the dwell. The hoop stresses during quenching and dwelling varied with the variation in HTC values. The difference in the three models, HTC1, HTC2, and HTC3, however, disappeared during annealing, and the three HTCs predicted the similar distribution at the end of the process, as shown in Figure 3-14 and Figure 3-16. The difference at the end of entire quenching process was minimally affected by varying the HTC values.

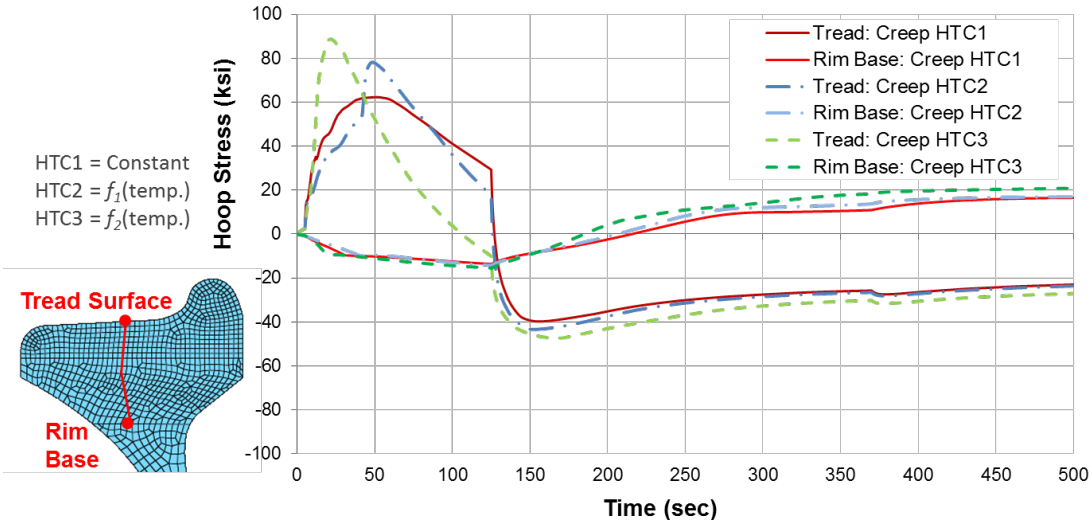

Figure 3-13. Time history of hoop stress during first 500 seconds of quenching process: HTC1, HTC2, and HTC3

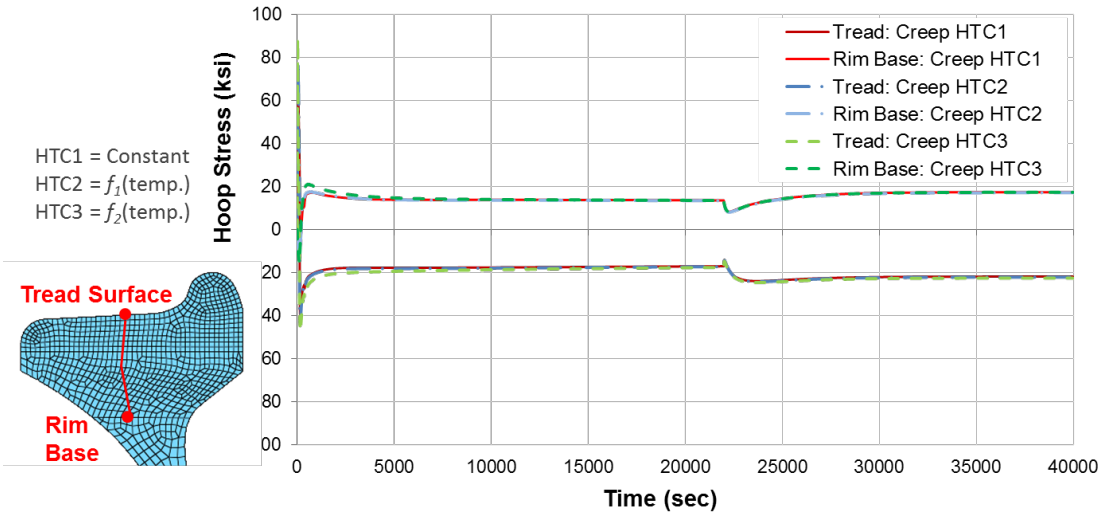

Figure 3-14. Time history of hoop stress during entire quenching process: HTC1, HTC2, and HTC3

At the end of the quench, the hoop stress on the tread surface varied with the value of HTCs, from -10.03 to 29.31 ksi (-69.15 to 202.09 MPa), as shown in Figure 3-15. It was caused by the different cooling rate depending on the HTCs applied in the heat transfer analysis. It resulted in the different trends of temperature and hoop stress during quenching. The difference in the trends between HTCs did not, however, affect the formation of microstructure desired in the wheel. As shown in Figure 3-16, the difference in the hoop residual stress at the end of entire process was less than 1 ksi (6.89 MPa) between HTCs, 0.23 ksi (1.59 MPa) for the rim base, and 0.67 ksi (4.62 MPa) for the tread surface, respectively.

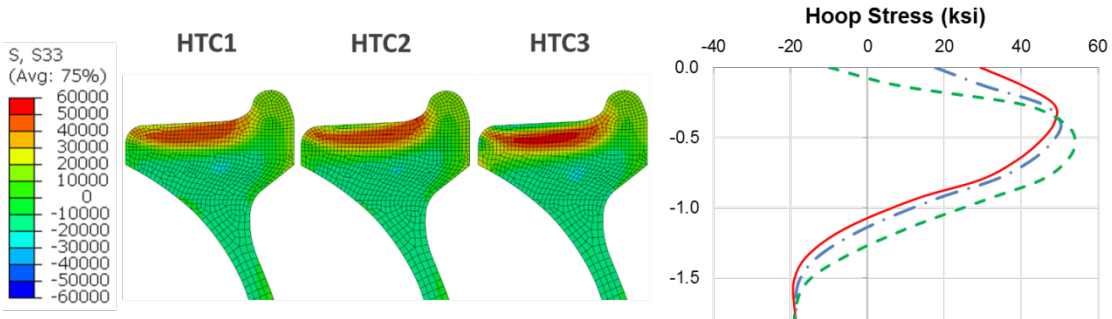

Location	Rim Base	Tread
HTC1	-14.72 ksi	29.31 ksi
HTC2	-14.27 ksi	17.52 ksi
HTC3	-15.44 ksi	-10.03 ksi

Figure 3-15. Hoop stress distribution in the section of wheel rim at the end of quench: HTC1, HTC2, and HTC3

The rim thickness for new wheel, a one-wear wheel, used in this study was 1.5 inches (3.81 cm). The condemning limit for the thin rim of wheel is 11/16 inch (1.75 cm). It means that a wheel with a rim free of cracks can remain in service until the rim has worn to a thickness of 13/16 inch

(2.06 cm). The compressive residual stress layer was approximately 1.1 inches (2.79 cm) deep from the tread surface; it is deeper than the 13/16 inch (2.06 cm) of allowable worn thickness in the wheel rim. After reaching the condemning limit, the compressive residual stress still remains near the tread surface of worn wheel. If it is assumed that the residual stress distribution remains unchanged from manufacturing during the life of the wheel, compressive hoop residual stress will still remain in the rim at the point when the wheel should be discarded.

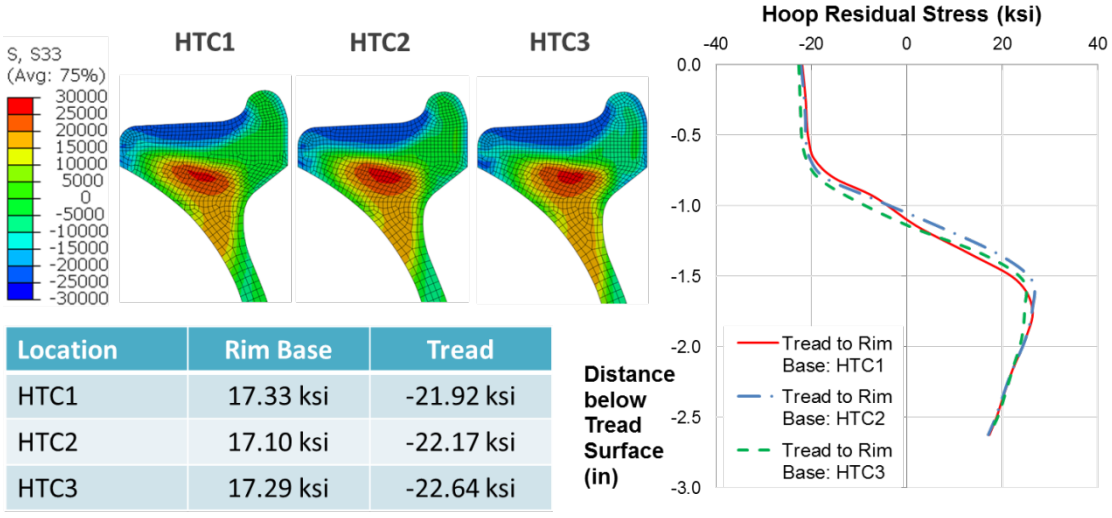

Location	Rim Base	Tread
HTC1	17.33 ksi	-21.92 ksi
HTC2	17.10 ksi	-22.17 ksi
HTC3	17.29 ksi	-22.64 ksi

Figure 3-16. Hoop residual stress distribution in the section of wheel rim at the end of process (cooling): HTC1, HTC2, and HTC3

3.5 Material Properties for Heat-Treated Wheel

As expected, the microstructure along the wheel section was changed after heat treatment; it resulted in desirable changes in the thermal and mechanical properties of wheel. For the subsequent thermal and mechanical analyses in this study, different thermal and mechanical material properties for the affected wheel areas were considered. These thermal and mechanical material properties were applied in two and three different regions, respectively, as shown in Figure 3-17.

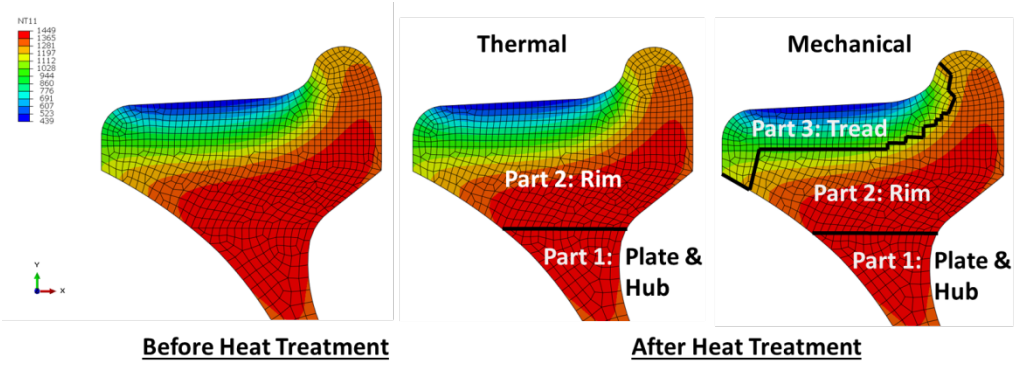

Figure 3-17. Regions with the different thermal and mechanical material properties before and after heat treatment [8]

The heat-treated material properties for the rim and the tread surface are presented in Figure 3-18. All material properties used in the analysis were extracted from the published data based on experimental results for Class C steel [8].

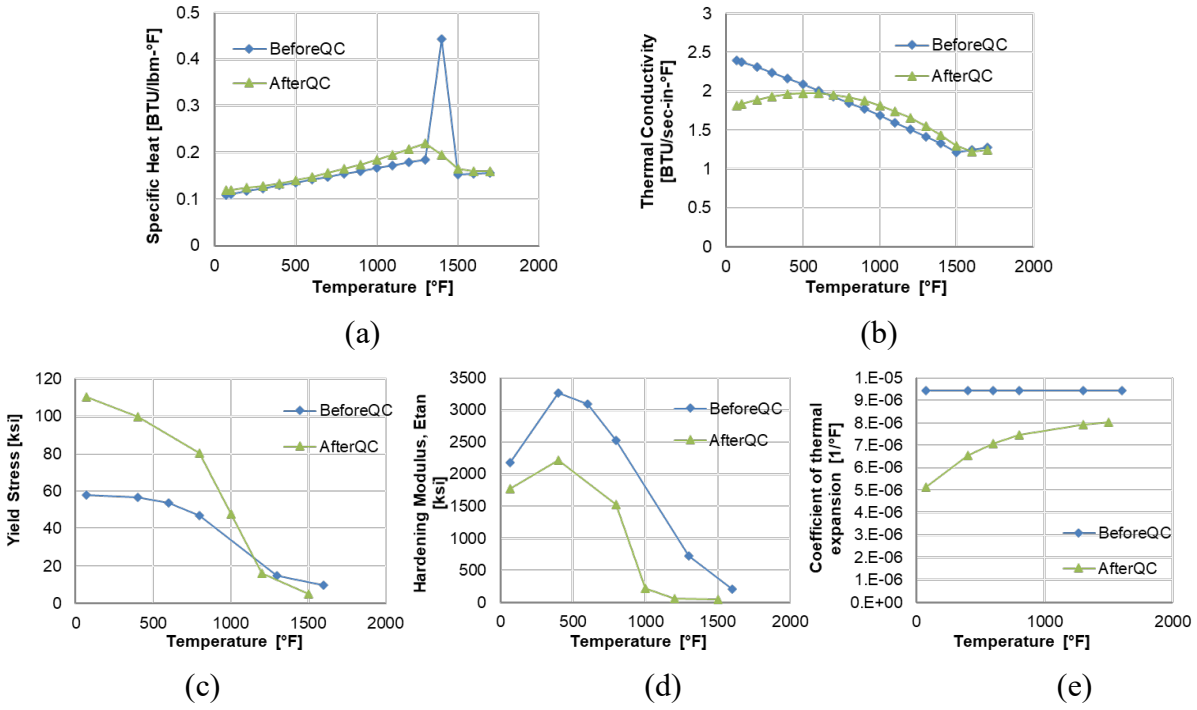

Figure 3-18. Thermal and mechanical material properties for the rim and tread surface after heat treatment: (a) specific heat, (b) thermal conductivity, (c) yield strength, (d) hardening modulus, and (e) coefficient of thermal expansion [8]

As shown in the figure, due to aging at room temperature, the yield stress of the rim, especially near the tread surface, increased after heat treatment, while the hardening modulus decreased. For the heat-treated material, the strength and hardness of the rim were finally higher than those of the plate and hub – because the plate and hub were least affected by the heat treatment. These heat-treated material properties were used in the following analysis for the service conditions of wheels.

4. Estimation of Residual Stress: Wheel and Rail Contact Loads

In this section, wheel performance analyses to determine the effects of in-service loads on the residual stress distribution are described.

4.1 Wheel and Rail Profiles

The elastic stresses at the wheel-rail interface are determined in this section. The vehicle is assumed to weigh 286,000-lbs (1,272-kN), which implies a static wheel load of 35,750-lbs (159-kN) applied to the 136 AREA rail. It is assumed that the 36-inches (91.44-cm) freight wheel with 1:20 tapered is running on the rail with 1:40 canted. The wheel used in this section is described in more detail in Section 3.1.2.

Contact locations to consider the stresses in the wheel rim were determined around the center of the tread where the thermal damage (shelling and spalling) is generally observed to occur [34]. Figure 4-1 presents the nominal contact position and loads between the wheel and the rail. The track gauge was 56.5 inches (1,435 mm), and the inside gauge of wheelset was 53 inches (1,348 mm).

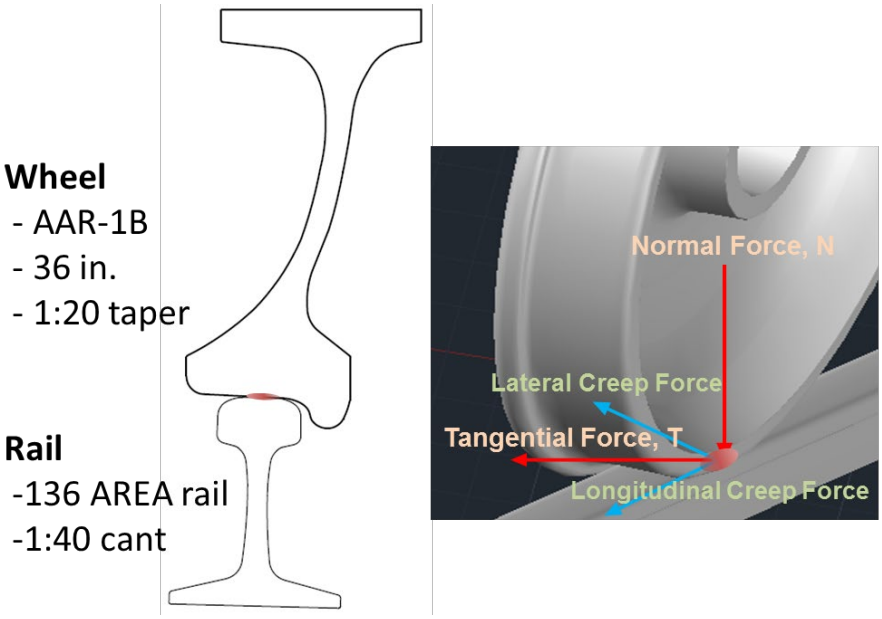

Figure 4-1. Wheel and rail contact configuration and contact loads

4.2 Wheel Load Environment

The traction loads generated under heavy braking and during curve negotiation result in accelerating the shakedown on the tread surface. Lateral wheel loads are exclusively generated under curving. Thus, a wheel in railroad service where curves are encountered relatively more in frequency and severity would experience longitudinal and lateral traction loads. These loads may be higher when wheel-rail conditions are dry, i.e., high friction coefficient.

Wheel and rail contact stresses were calculated for three different traction coefficients: 0.00, 0.29, and 0.39. The contact loads were calculated for a train speed of 40 mph (64.4 km/h) which was the balance speed in the curve being considered.

As shown in Figure 4-1, two loads, normal (vertical) and tangential, developed from the contact between the wheel tread and the rail. The normal (vertical) force, *N*, was induced by the weight of vehicle on the supported rail. The tangential force, *T*, was the resultant of longitudinal and lateral forces. The contact loads used in this study are shown in Table 4-1.

Table 4-1. Wheel and rail contact loads environment

Vertical [kip]	Lateral [kip]	Longitudinal [kip]	Tangential [kip]	μ (=*T*/*N*)
35.750	0.000	0.000	0.000	0.000
35.750	8.938	5.363	10.423	0.292
35.750	8.938	10.725	13.961	0.391

4.3 Wheel and Rail Contact Model

The contact between wheel and rail is classified into two conditions: one- and two-point contact. For one-point contact, when the train is running on a straight (tangent) track, the contact typically occurs at a single point on the tread of the wheel. On the other hand, if the wheelset experiences a lateral displacement while negotiating curves or due to lateral track defects, such as narrow gage or severe alignment, there can be two points of contact: on the tread and on the flange of the wheel.

The tangential forces in flange contact cause the wheel to wear rather than develop RCF. RCF damage on wheels is severe usually toward the field side of the wheel from the tape line [35]. This study focuses on contact positions outside of the point which is 0.5 inch (13 mm) toward the flange from the tape line.

4.3.1 Wheel and Rail Contact Location

As mentioned above, a single point of wheel and rail contact on the wheel tread is considered a function of the lateral relative displacement, which is lateral shift. To define the contact location, a fixed coordinate system is considered with the origin at the center of wheelset on the track centerline. The x-axis is the rolling direction, along the tangent to the track centerline; the z-axis is vertically upward as a positive direction; and the y-axis is the transverse direction of wheel section with positive movement from left to right.

The location of wheel and rail contact depends on the geometry and profiles of wheel (AAR-1B) and rail (136 AREA rail). It is determined from specified wheel and rail profiles and lateral displacement of the wheelset. In this study, the wheel and rail contact data were determined by using MATLAB [36]. The results of contact data were verified by comparing to those from VAMPIRE® [37]. The possible locations of the wheel and rail contact model used in this study are presented in Figure 4-2. Consistent with the contact location, the rolling radius of the wheel and the contact angle were computed. In this study, the relative lateral axle displacement ranged

± 0.3 inch (± 7.6 mm). This range is generally considered the contact location with the wheel traveling on tangent track.

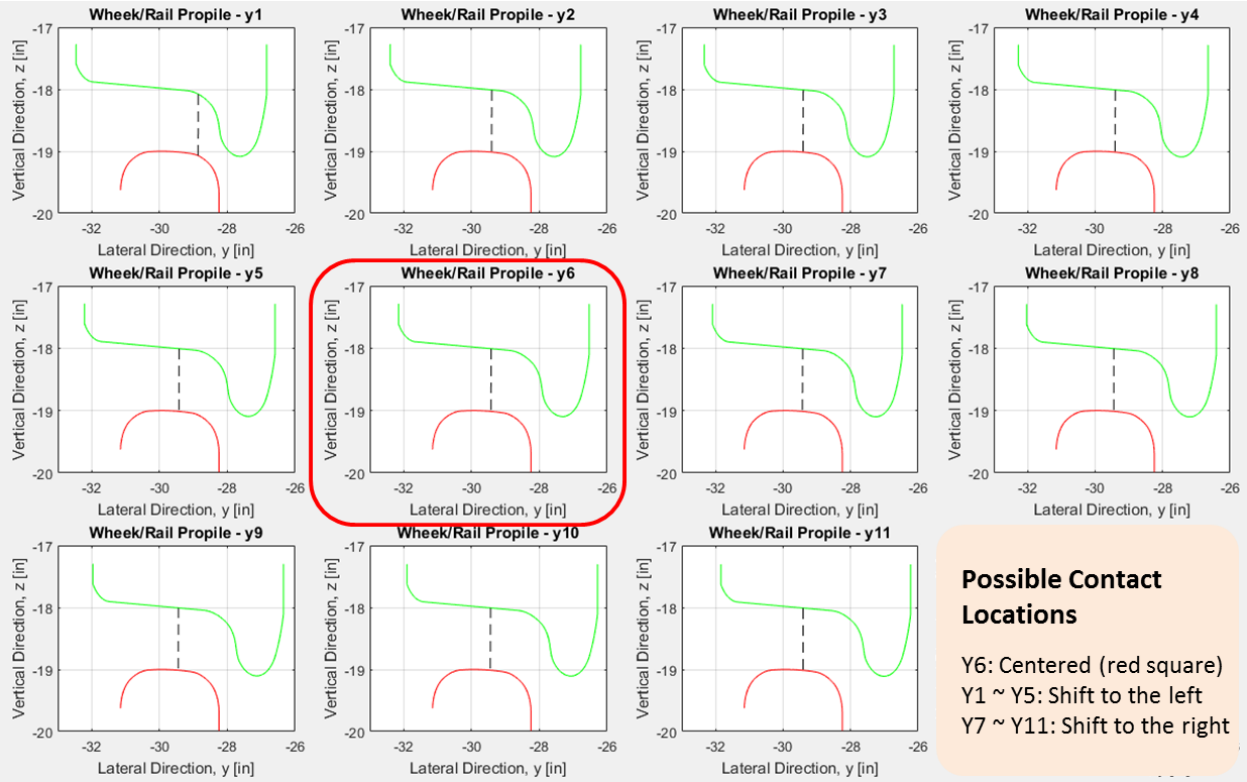

Figure 4-2. Possible wheel and rail contact locations determined in MATLAB

4.3.2 Normal Pressure and Traction in the Wheel and Rail Contact Area

The distribution of the contact pressure and traction in the wheel and rail contact was determined by using CONTACT [12]. This program calculates surface traction and contact geometry boundary conditions with given material properties, speed, or creepages.

In general, to obtain a contact geometry boundary, the theory of elastic contact by Hertz [11] is used. As the contact problem is localized, two bodies come in contact with each other and the point where the first contact occurs is the origin.

The contact area is assumed to be elliptical close to the origin into contact, as shown in Figure 4-3. The pressure distribution, p, on the elliptical contact area, A_c, is described by the quadratic equation as follows:

$$p(x,y) = p_0\sqrt{1-\left(\frac{x}{a}\right)^2-\left(\frac{y}{b}\right)^2}, \qquad (x,y) \in A_c \tag{4.1}$$

Where,

a and b	are the semi-axes of the elliptical contact area,
p_0	is the maximum pressure, and
x and y	are the coordinates within the elliptic area.

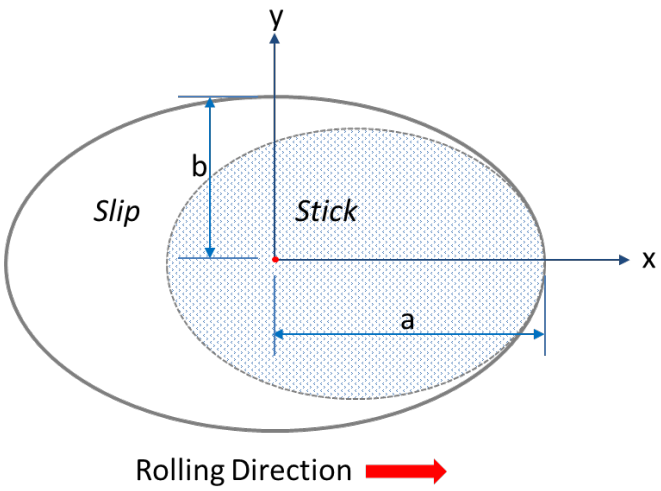

Figure 4-3. Elliptical contact area

The semi-axes for the contact patch in Figure 4-3 can be calculated under a predefined vertical load condition.

The procedure in CONTACT is based on the discretization of the potential contact area. Based on the semi-axes of the elliptical contact area, the potential contact area is introduced as a rectangular area within the contact plane containing at least all wheel and rail contact. The area is divided into the smaller size of rectangular elements. Normal pressure and traction are constant in the rectangular elements. Some creep is expected when a wheel in rolling contact is subjected to traction. If the two bodies (wheel and rail) have a relative motion, the contact area will slip between two bodies. If not, the area will stick between the contacting bodies. Creep increases as the slip portion of the contact area increases.

Contact stresses under varying normal (vertical) and tangential force conditions were simulated by accounting for a partial slip-stick (adhesion) phenomenon. Surface traction state, slip, and adhesion (stick) regions were determined for the three load environments provided in Table 4-1. Each environment was simulated with and without spin creep resulting in six representative cases: NT1 to NT6. Figure 4-4 shows the resulting stick and slip regions. Cases NT4 to NT6 included the spin creepage produced from the contact configuration of the wheel and rail profile and position in addition to the lateral and longitudinal creepage. Figure 4-5 presents the results of normal pressure and traction for the six cases.

As shown in Figure 4-4 and 4-5, including the spin creepage reduced the stick portion on the contact area. At the same time, it produced negative lateral and longitudinal traction due to the angle between the wheel and rail profiles in contact.

The normal pressure and surface traction in the wheel and rail contact zone determined from CONTACT were used in the stress analysis as an input for the loading condition.

NT1: Contact Ψ1-1
Ψ = 0.0
N = 35.75 kip Lateral = 0 kip
μN = 14.3 kip Longitudinal = 0 kip
μ = 0.4 T = 0 kip

NT2: Contact Ψ1-2
Ψ = 0.0
N = 35.75 kip Lateral = 8.9 kip
μN = 14.3 kip Longitudinal = 5.4 kip
μ = 0.4 T = 10.4 kip

NT3: Contact Ψ1-3
Ψ = 0.0
N = 35.75 kip Lateral = 8.9 kip
μN = 14.3 kip Longitudinal = 10.7 kip
μ = 0.4 T = 14.3 kip

NT4: Contact Ψ2-1
Ψ = 0.00303
N = 35.75 kip Lateral = 0 kip
μN = 14.3 kip Longitudinal = 0 kip
μ = 0.4 T = 0 kip

NT5: Contact Ψ2-2
Ψ = 0.00303
N = 35.75 kip Lateral = 8.9 kip
μN = 14.3 kip Longitudinal = 5.4 kip
μ = 0.4 T = 10.4 kip

NT6: Contact Ψ2-3
Ψ = 0.00303
N = 35.75 kip Lateral = 8.9 kip
μN = 14.3 kip Longitudinal = 10.7 kip
μ = 0.4 T = 14.3 kip

Figure 4-4. Evolution of stick and slip regions in the wheel and rail contact area with the various traction coefficients determined by CONTACT

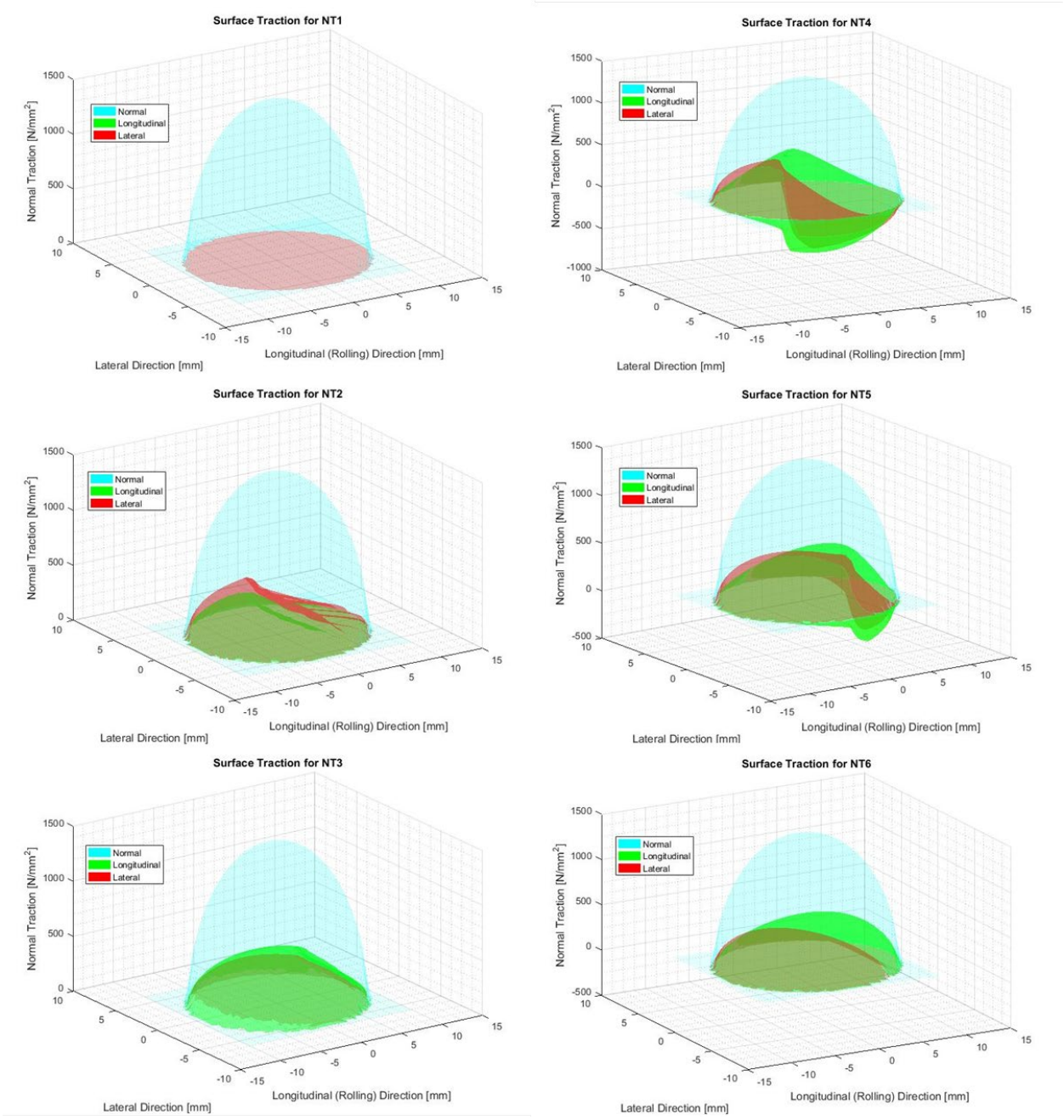

Figure 4-5. Normal pressure and traction on the wheel and rail contact area determined by CONTACT [MPa, mm]

4.4 Residual Stress Estimation after Removing Wheel and Rail Contact Loads

The Abaqus FEA program was used to calculate the changed stress-strain environment in the wheel when the contact forces were combined with the existing residual stresses from the manufacturing process.

The FE model for wheel and rail contact simulation was the same as the model used in estimating the residual stress from the manufacturing process. The residual stresses from the

manufacturing process were used as the initial stress condition. The material properties used were considered as heat-treated material, as shown in Figure 3-18.

The variables considered for the stress analysis for wheel rail contact loads were:

(1) Three different traction coefficients

(2) With and without spin creepage

The values of the pressure and traction used are shown in Figure 4-4.

The shape of the contact area considered was an elliptical in the CONTACT simulation. However, the surface of the 3D element in the FE model was a rectangular shape. Based on the approach outlined in [11], the normal pressure and traction distributions shown in Figure 4-5 were converted to inputs that conformed with the discretized contact area in the FE model. Figure 4-6 shows the contours for von Mises stress under the wheel and rail contact loads.

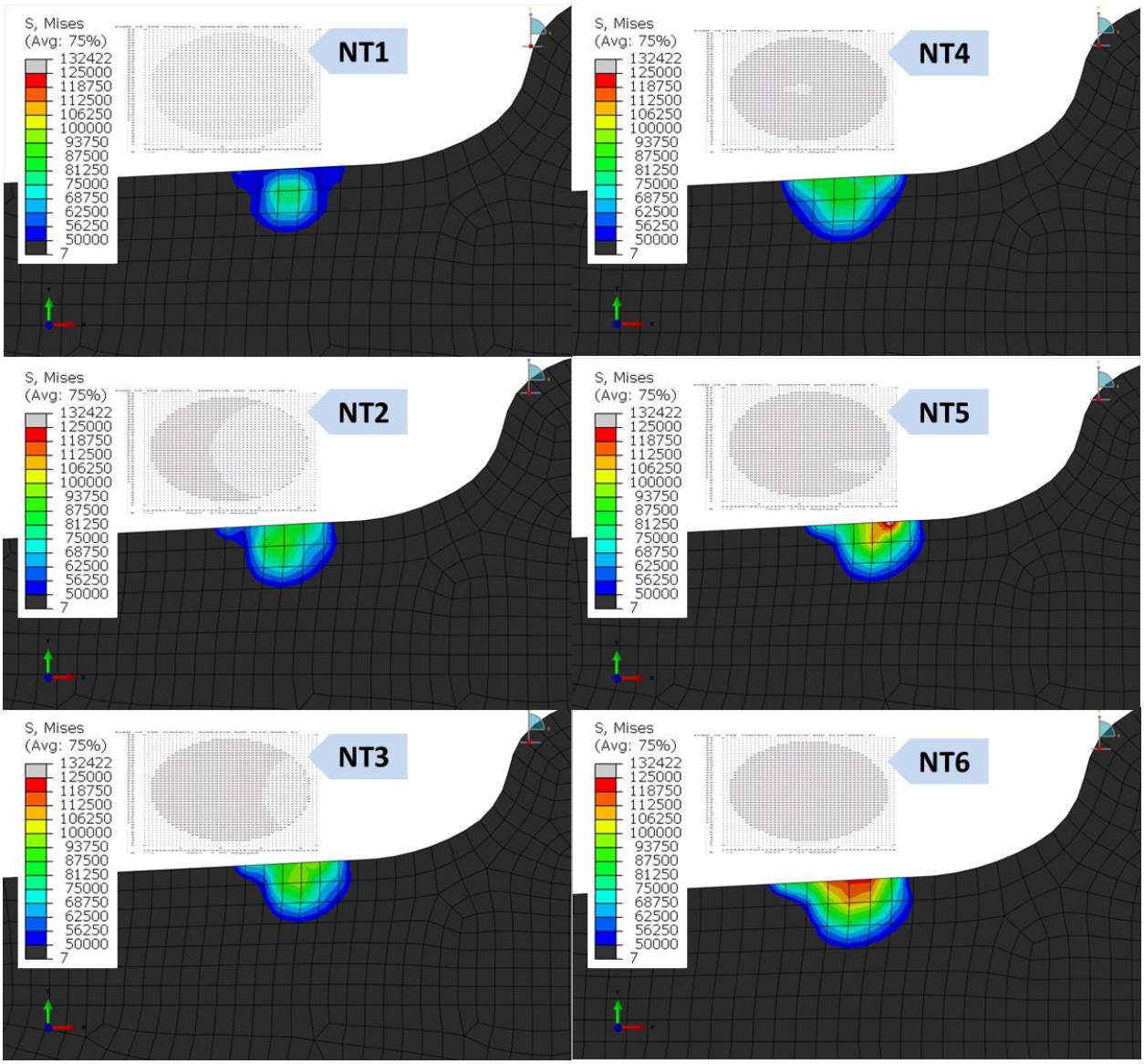

Figure 4-6. Contour plot for von Mises stress under the contact loads [psi]

The hoop stress results with and after removing the contact loads are presented in Figure 4-7 and 4-8, respectively.

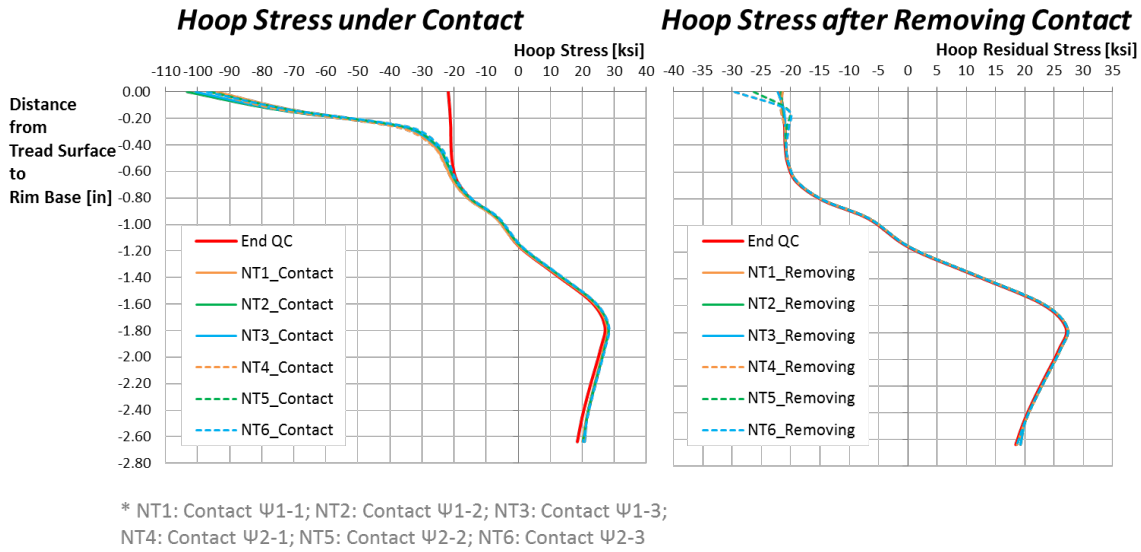

* NT1: Contact Ψ1-1; NT2: Contact Ψ1-2; NT3: Contact Ψ1-3; NT4: Contact Ψ2-1; NT5: Contact Ψ2-2; NT6: Contact Ψ2-3

Figure 4-7. Hoop stress results under and after removal of the wheel and rail contact loads and rail contact loads

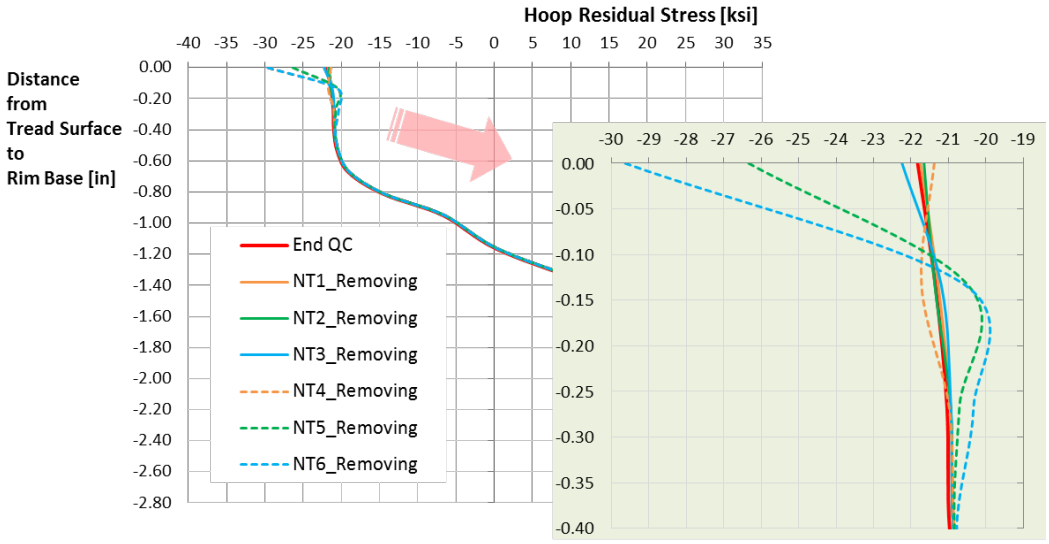

Figure 4-8. Detail of hoop residual stress distribution after removing the wheel and rail contact loads

With contact loads, the hoop stress at the tread surface for all cases varied from -97 to -84 ksi (-669 to -579 MPa). NT3 was the only case that yielded at the surface under contact load, since the compressive hoop stress at the surface was less than that at the subsurface (immediately below tread surface). The NT6 load case, which shows the stress state near yield, included high tractions and spin creep likely to be present under contact angle and/or high angle-of-attack conditions such in sharp curves.

After removing the contact loads, the residual stress distribution was modified. It was apparent that the effect of contact stresses was confined to a region very near the wheel tread surface, depending on the traction coefficient. As the traction coefficient increased (NT5 and NT6), the compressive residual stress also increased at the tread surface and the subsurface immediately below.

For load cases of NT1, NT2 and NT3, normal and tangential (traction) forces without spin creepage, and load case of NT4, normal force with spin creepage, the hoop residual stress changed minimally, within ± 2.5 percent. For these four cases, the hoop stress distribution 0.4 inch (10 mm) below the tread surface remained unchanged.

5. Estimation of Residual Stress: Thermal Load Due to Tread-braking

The hoop residual stresses in the as-manufactured wheel rim are expected to last for a significant period under normal braking service. This section describes the effects of normal service and possible extreme braking conditions on the residual stress.

5.1 Thermal Load Condition from Tread-Braking

Brakes are used to control train speed and bring the train to stop under normal as well as emergency conditions. Tread-braking is the traditional mechanical braking system used for freight trains. Pressing the brake shoe against the wheel tread by the forces generated by the train airbrake system leads to the heating of the wheel due to friction at the shoes and wheel interface. Figure 5-1 shows a schematic of the concept of wheel tread-braking.

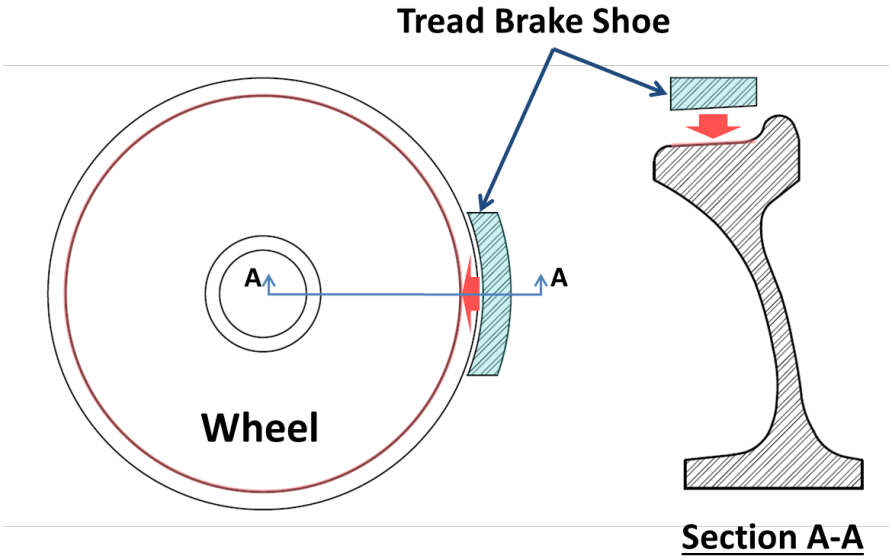

Figure 5-1. Wheel tread-braking schematic

5.1.1 Drag-Braking

Drag-braking is commonly used while trains descend a long grade to control the speed of the train for a relatively longer duration compared to stop-braking. It also occurs when brakes fail to release. As a result, the brake shoe continues to press against the wheel tread, generating heat and raising the wheel tread temperature beyond the range normally seen in service applications. Another situation where wheels can get over-heated is when the handbrakes on car(s) are left applied by mistake. Unless promptly detected, this causes the wheel tread to heat up and can result in the removal of the damaged wheel from service.

For drag-braking analysis, AAR S-660 [27] specifies an input of 38 horsepower (HP) for 20 minutes as a thermal load with the resulting heat flux is evenly applied over the tread surface of the wheel. To cover an extreme horsepower case, 50 HP was also considered in this study. This case is not unreasonable, as significant variations in wheel temperature have been observed –

even in unit trains with a uniform braking system under normal braking applications. 50 HP is within reason since different braking levels are achieved between cars in a train, as much as 50 percent higher on many wheels than the mean for the entire train.

The simulation matrix for drag-braking is shown in Figure 5-2. Three different braking durations of 20, 30, and 40 minutes were considered for thermal load of 38 HP; 20 minutes was considered for thermal load of 50 HP.

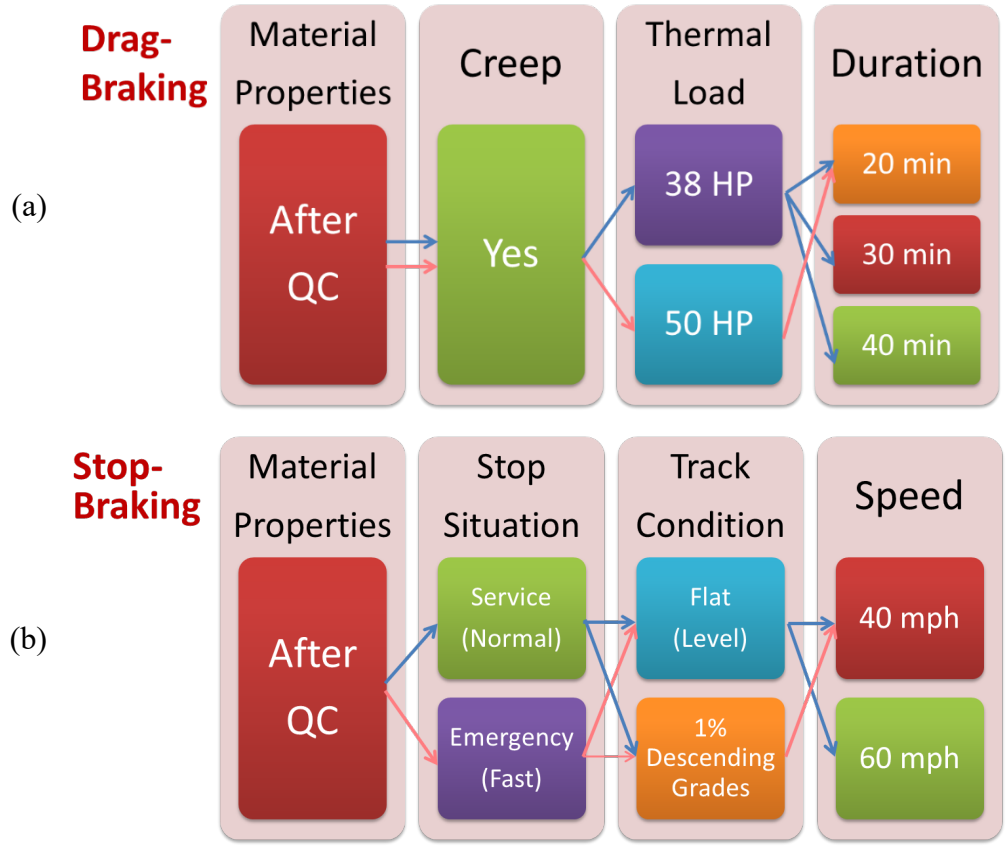

Figure 5-2. Simulation matrix for (a) drag-braking and (b) stop-braking

5.1.2 Stop-Braking

The brake application for full-service stops requires a brake pipe pressure reduction of 26 psi (179 kPa). Although the corresponding brake shoe force and hence the heat input rate into the wheel is higher than the drag-braking case, the full-service application for stop braking does not last as long.

The stop-braking scenarios for the freight train were simulated by the Train Energy and Dynamics Simulator (TEDS) [38] for various stop situations, track conditions, and speed. The conditions for stop-braking as shown in Figure 5-2 were:

- Level tangent: service and emergency stops from 40 and 60 mph
- 1 percent descending grade: service and emergency from 40 mph.

For each combination of conditions, the detail information on the maximum braking HP, and the associated timing is listed in Table 5-1.

Table 5-1. Train Stop-Braking Simulation Results from TEDS

		Maximum HP [hp]	Time at the Maximum HP [sec]	Time when stopped [sec]
Level Track	FF 40 mph	85.5	38	84
	FF 60 mph	133	41	111
	EF 40 mph	135.9	13	49
	EF 60 mph	206.2	14	72
1% Descending Grade Track	F1% 40 mph	107.2	46	116
	E1% 40 mph	145.9	14	63

* FF: Full service stop on level tangent (Flat); EF: Emergency stop on level tangent (Flat); F1%: Full service stop on 1% downhill; E1%: Emergency stop on 1% downhill.

5.2 Finite Element Analysis

To determine residual stress distribution in the wheel after the tread-braking, transient thermal analysis was used to calculate the temperature distribution in the wheel as a function of time. This was followed by a stress analysis for the duration of the braking and the time for the wheel to return to ambient temperature.

For the tread-braking simulation, the three-dimensional model of the wheel developed for the manufacturing process was used to conduct a decoupled thermo-mechanical analysis to determine the residual stress from service braking. Transient HTA was conducted to obtain the time history of the temperature distribution in the wheel. The output temperature distribution history in the wheel model was then used as an input (i.e., thermal loads) to the stress analysis.

5.2.1 Heat Transfer Analysis

The heat flux used for thermal analysis was a constant value under drag-braking for the entire 20 minutes. The heat flux input was a time-dependent function of brake horsepower (computed based on the brake shoe friction force and the train speed) for stop-braking. The heat flux was applied to the contact region at the wheel tread and the brake shoe interface, as shown in Figure 5-1. The width of thermal load application specified in AAR S-660 [27] was adopted in the heat transfer analysis: the width was 3-3/8 inches (85.7 mm), and the brake shoe center line was placed on a distance of 3-7/16 inches (87.3 mm) from the face of the back rim.

The thermal properties for various regions of the wheel sections shown in Figure 3-17 were used. The values of these properties as function of temperature are plotted in Figure 3-18. Except for the heat flux input area, a constant value of 5.0 Btu/hr-ft^2-°F (28 W/m^2) for the HTC was used on the entire wheel surface.

5.2.2 Stress Analysis

After the heat transfer analysis, using the temperature distribution history, the simulation continued to estimate the residual stresses resulting from the brake application.

The stress analysis used the temperature dependent mechanical properties shown in Figure 3-18, which were applied in the three different regions of the wheel shown in Figure 3-17.

5.3 Residual Stress Modification due to Tread-braking

This section presents the results of the FE simulation for the thermal loads due to tread-braking and discusses how tread-braking and the resulting heating of the wheel can lead to changes in the residual stress distribution imparted during the manufacturing process.

5.3.1 Heat Transfer Analysis

As shown in Figure 5-2, the heat transfer analyses were conducted for tread-braking as follows:

(1) Drag-braking: 38 HP for 20, 30, and 40 minutes and at 50 HP for 20 minutes

(2) Stop-braking: 6 scenarios from the combination of stop situation, track condition, and speed

For the drag-braking, the contour plot of maximum temperature distribution on the wheel section is shown in Figure 5-3. The time history of temperature distribution on the tread surface and rim base of the wheel for drag-braking is presented in Figure 5-4 and 5-5.

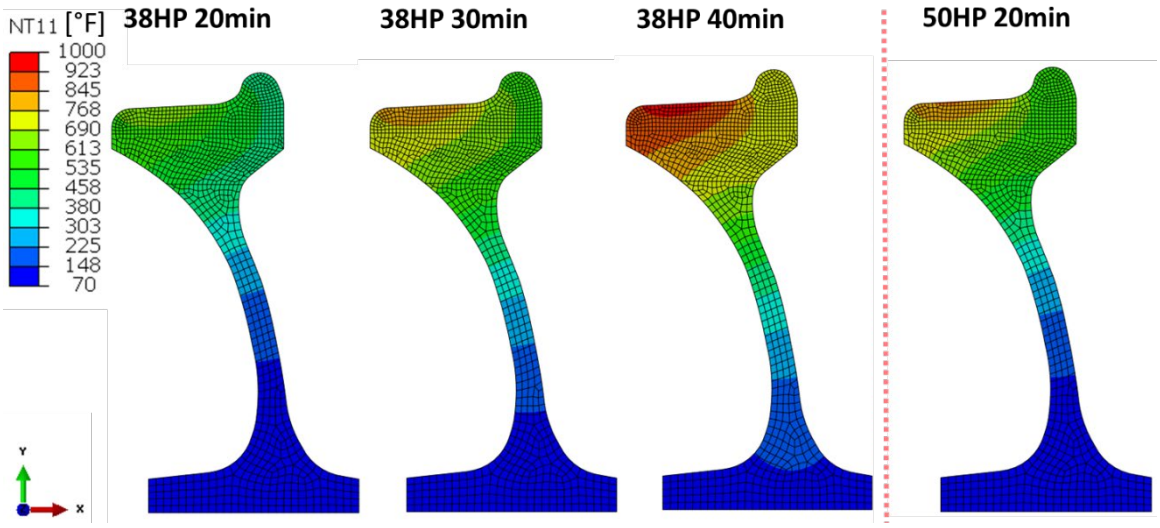

Figure 5-3. Contour plot of maximum temperature distribution on the cross-section of the wheel due to drag-braking

At the beginning of the drag brake application, the temperature on the tread surface increased more rapidly than that on the rim base. This means the tread surface of the wheel was expanded. The increase in rate of temperature depended on the magnitude of thermal input, as shown in Figure 5-5.

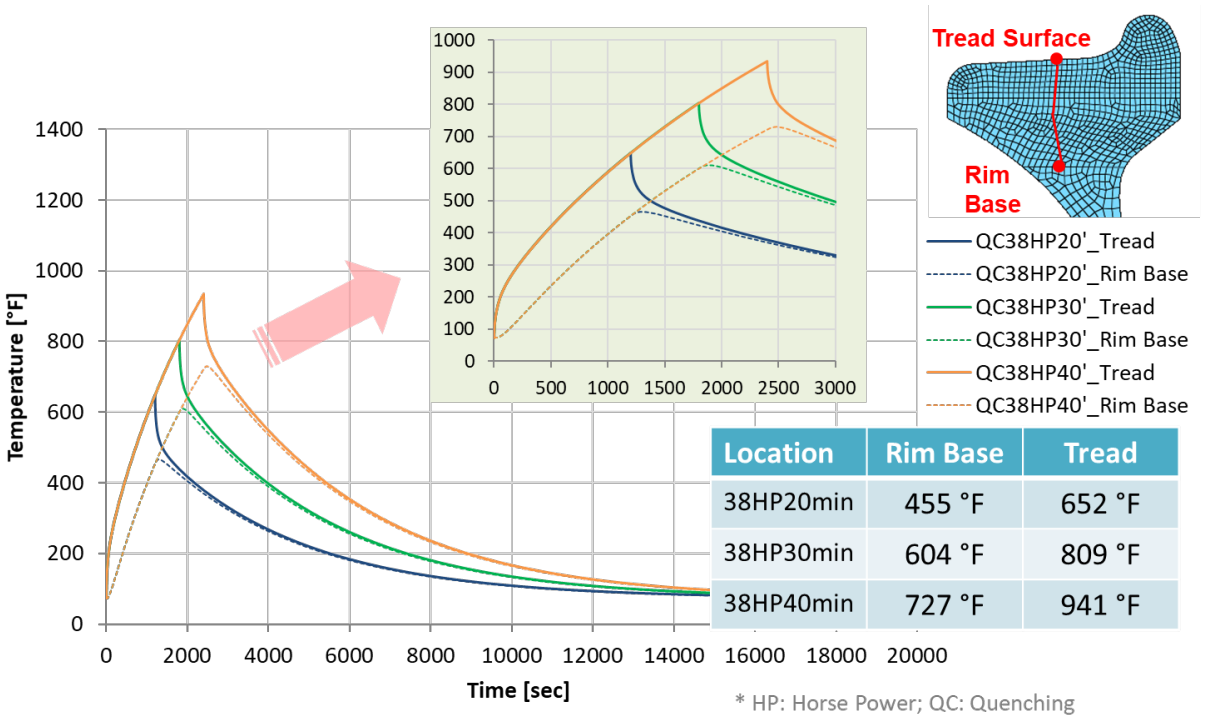

Location	Rim Base	Tread
38HP20min	455 °F	652 °F
38HP30min	604 °F	809 °F
38HP40min	727 °F	941 °F

Figure 5-4. Time history of temperature distribution for drag-braking: 38 HP for 20, 30, and 40 minutes

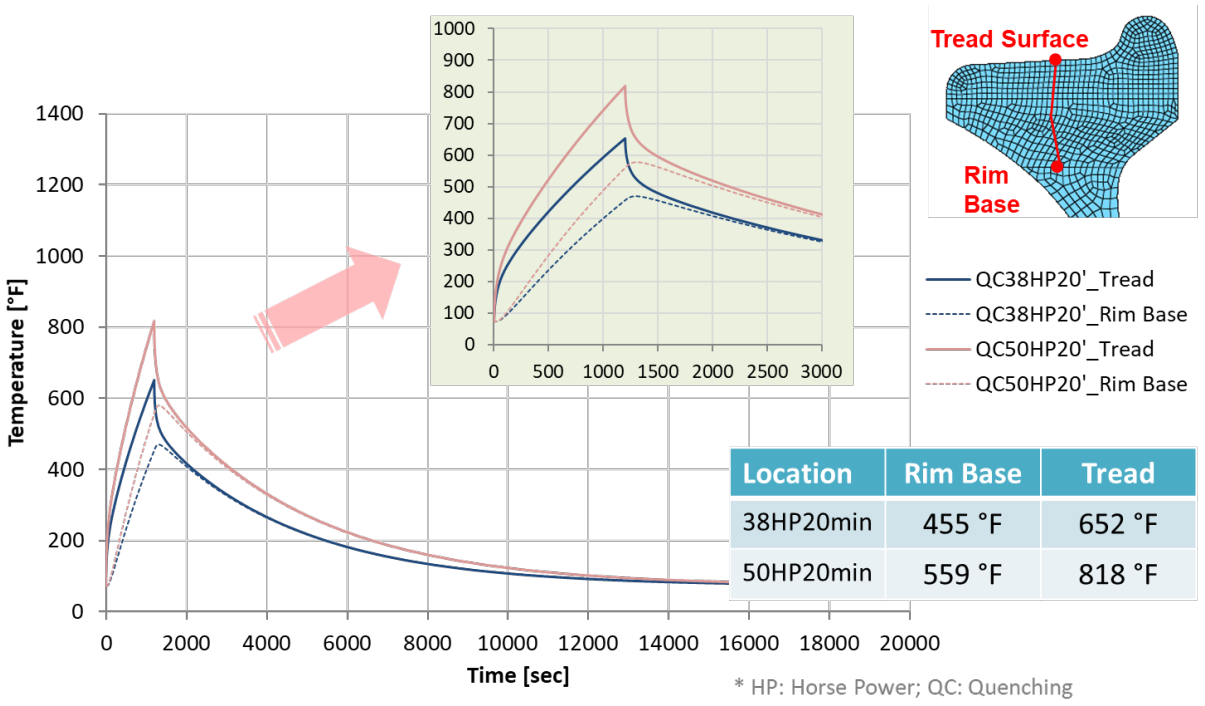

Location	Rim Base	Tread
38HP20min	455 °F	652 °F
50HP20min	559 °F	818 °F

Figure 5-5. Time history of temperature distribution for drag-braking: 38 HP and 50 HP for 20 minutes

For the 38 HP case, the maximum temperature at the tread surface was 652 °F (344 °C), 809 °F (432 °C), and 941 °F (505 °C) for each braking duration: 20, 30, and 40 minutes.

For the 50 HP case, the maximum temperature at the tread surface was 818 °F (437 °C) for the brake application of 20 minutes. During the cooling phase, the tread surface cooled first and the temperature decreased more rapidly than the rim base temperature.

For stop-braking, the contour plot of temperature distribution on the wheel section is presented in Figure 5-6 for the time when the temperature on the tread surface was at its maximum during the braking period. Figure 5-7 presents the time history of temperature distribution for six scenarios of stop-braking.

The temperature on the tread surface for the stop-braking dramatically increased in a very short period compared to the drag-braking (38 HP for 20 minutes), where the maximum temperature was reached at the end of 20 minutes. That is because the maximum horsepower for stop-braking ranged from 85.5 HP (FF 40 mph) to 206.2 HP (EF 60 mph). These values were much greater than the drag-braking at 38 HP, where the ratio of stop to drag-braking increased from 225 percent to 543 percent.

Stopping a train from a higher speed and on a descending grade requires a longer braking period. In addition, the emergency brake application case results in 20 percent higher brake horsepower than the full normal service application.

It is apparent that stop-braking tends to heat up the near tread surface of wheel rim as shown in Figure 5-6. Whereas in the case of drag-braking, the temperature increased in the tread surface and extended into the plate region, as shown in the temperature distribution on the cross-section of wheel, Figure 5-3. For drag-braking, when the tread surface reached the maximum temperature, the rim base had a temperature 25 to 30 percent lower than the tread surface. On the other hand, for stop-braking, the rim base remained at or around ambient temperature, due to the significantly different duration of the braking load.

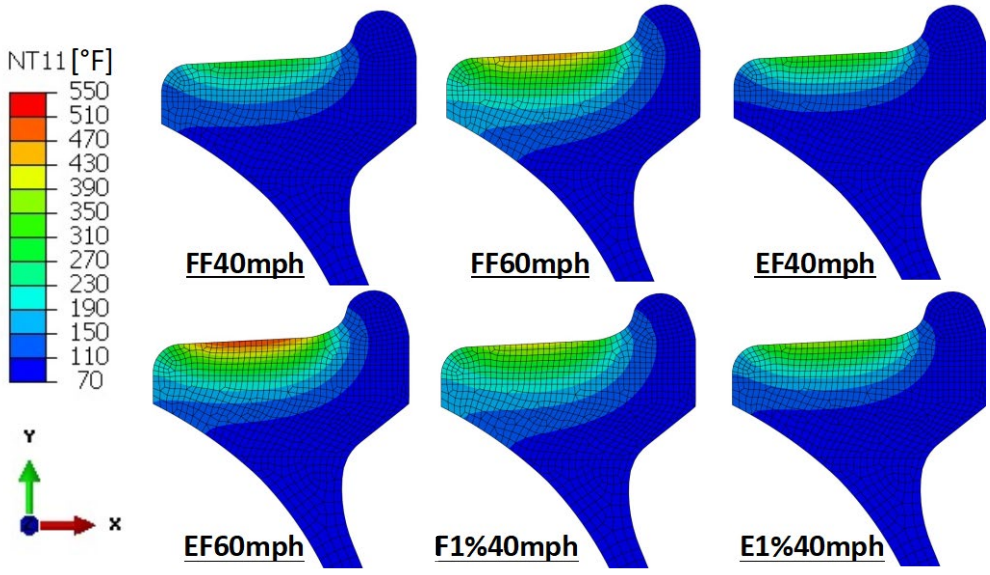

Figure 5-6. Contour plot of maximum temperature distribution on the cross-section of the wheel due to stop-braking

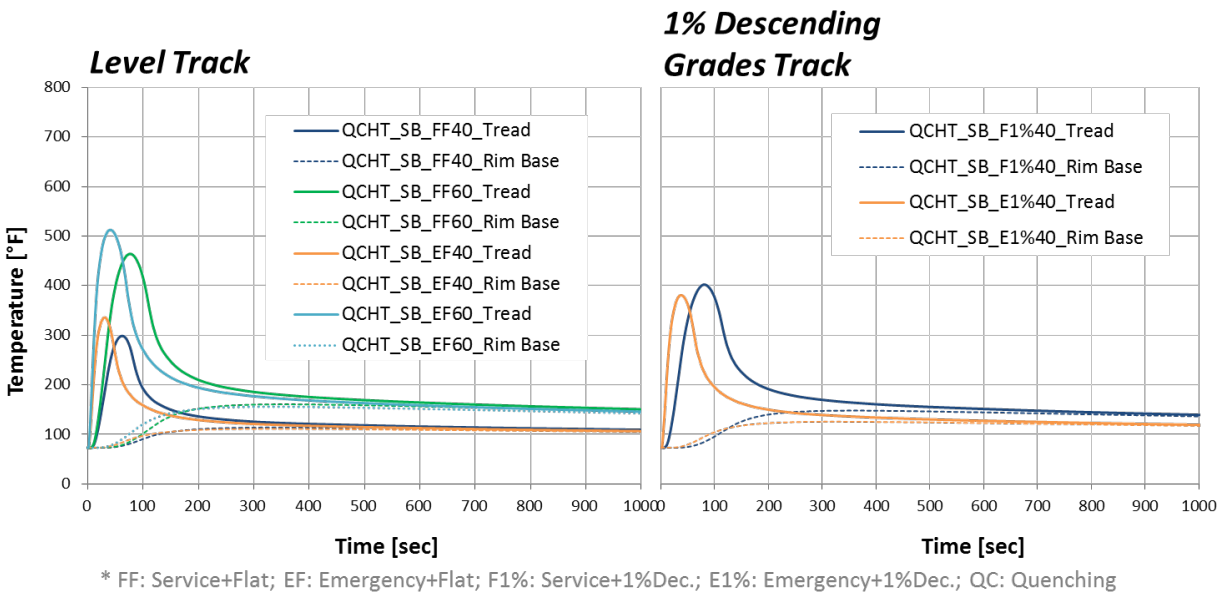

Figure 5-7. Time history of temperature distribution for six scenarios of stop-braking: (a) level track and (b) 1% descending grades track

Thermal loading under service conditions can develop high temperatures in the wheel rim. It may be possible that the development of temperatures above the austenitizing temperature lead to metallurgical transformation in the material. This transformation produces a brittle material at the tread surface due to the formation of martensite. It is clear, however, that the temperature in the rim during normal service braking did not reach the austenite phase.

5.3.2 Stress Analysis

The temperature distribution from the heat transfer analysis was used to determine the residual stress due to the tread brake application. The results of the stress analysis for three different durations for the drag-braking (38 HP) and a case of higher (50 HP) with the same duration as the standard drag-braking (20 minutes), are presented in Figure 5-8, 5-9, 5-10, 5-11, and 5-12.

The contour plot of hoop residual stress distribution on the wheel section for these four cases is presented in Figure 5-8. The time history of hoop stress distribution on the tread surface and rim base of the wheel is presented in Figure 5-9 and Figure 5-11.

At the beginning of braking, the compressive stress on the tread surface increased rapidly with the rise in temperature. Then, after reaching the maximum compressive stress, the compressive hoop stress on the tread surface dramatically decreased. The maximum value of compressive hoop stress depended on the magnitude of thermal input (heat flux and duration), e.g., as shown in Figure 5-9. The residual stresses on the tread surface depended on the duration of the brake application.

With a thermal input of 50 HP and the same duration of 20 minutes as shown in Figure 5-11, the maximum compressive hoop stress was less (closer to zero) than with the 38 HP thermal input.

These results show that the braking duration for stress reversal from compressive to tensile in the rim with thermal loads of 38 HP and 50 HP was approximately 35 and 20 minutes, respectively.

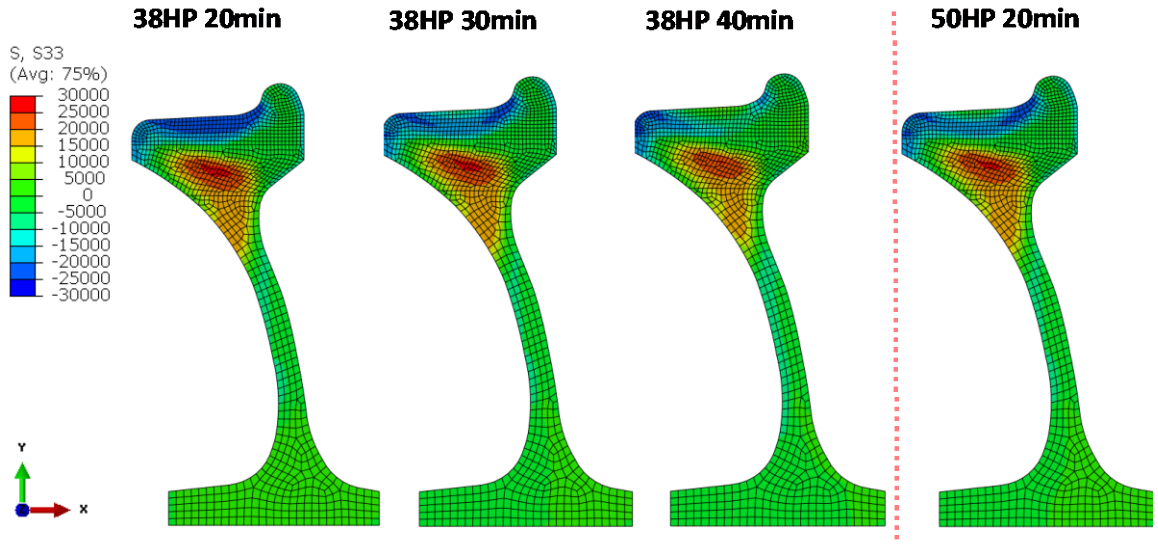

Figure 5-8. Contour plot of hoop residual stress distribution on the cross-section of the wheel for drag-braking [psi]

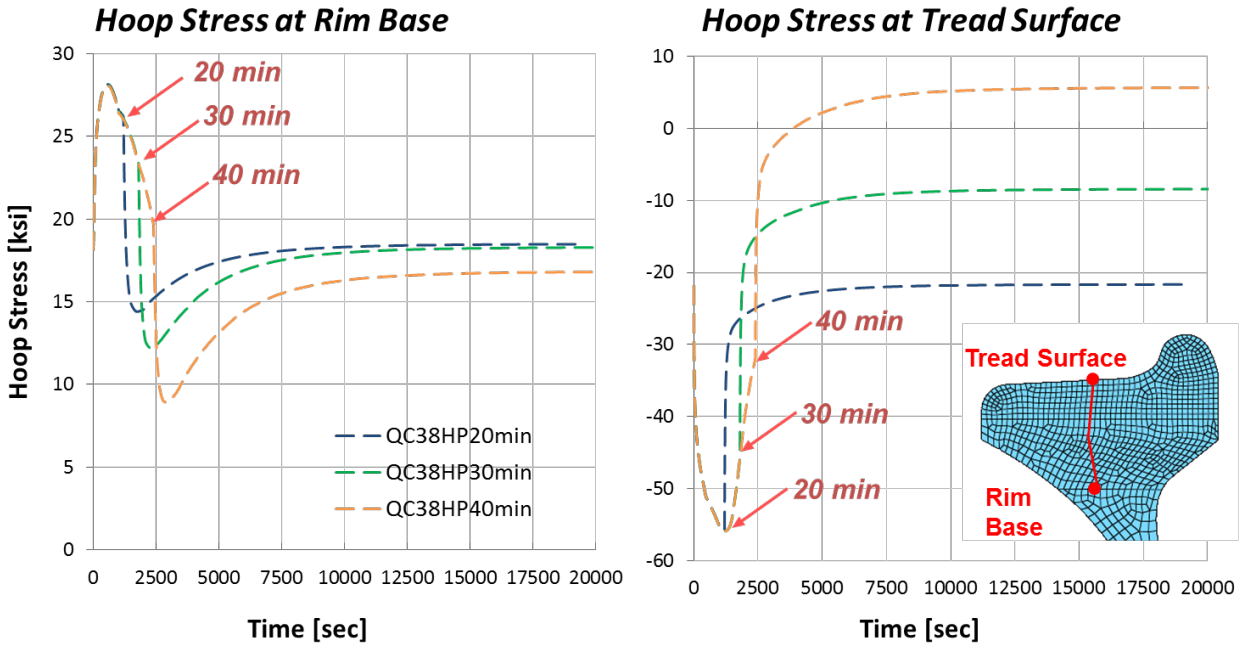

Figure 5-9. Time history of hoop stress distribution for drag-braking: 38 HP for 20, 30, and 40 minutes

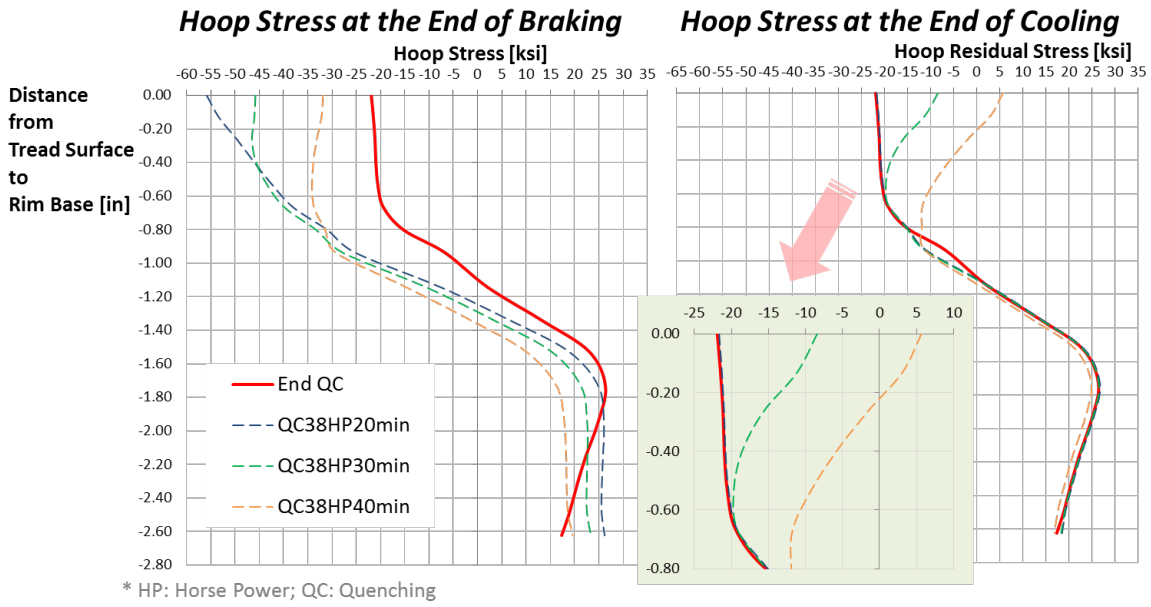

Figure 5-10. Hoop stress distribution on the cross-section of the wheel due to drag-braking: 38 HP for 20, 30, and 40 minutes

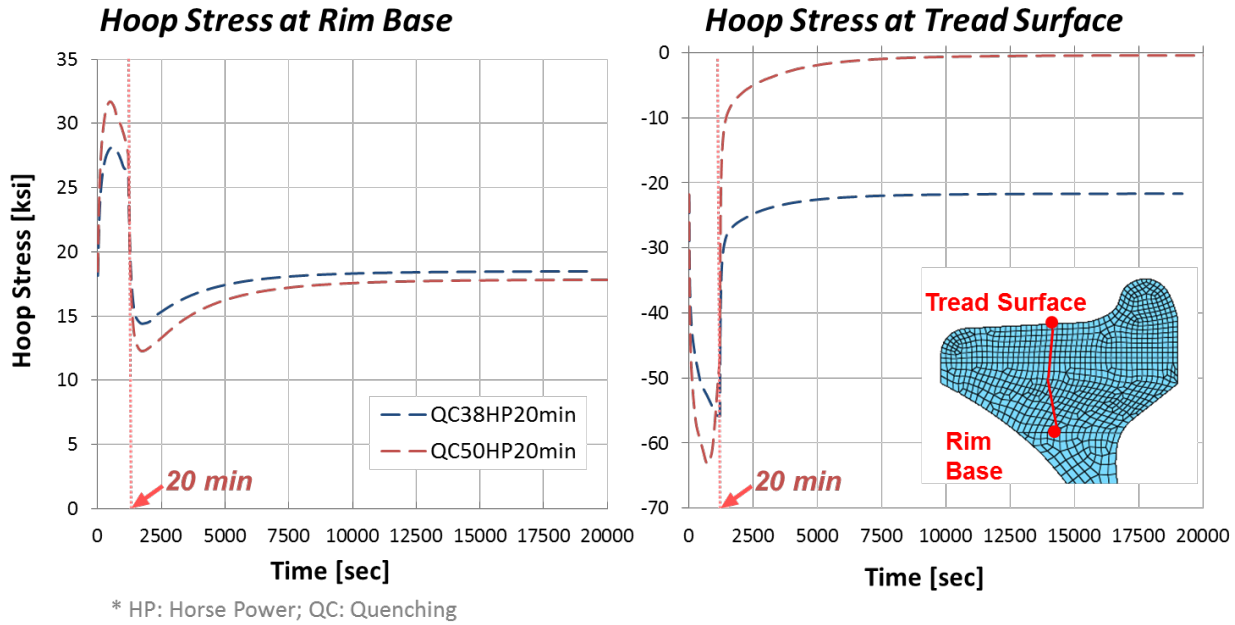

Figure 5-11. Time history of hoop stress distribution for drag-braking: 38 HP and 50 HP for 20 minutes

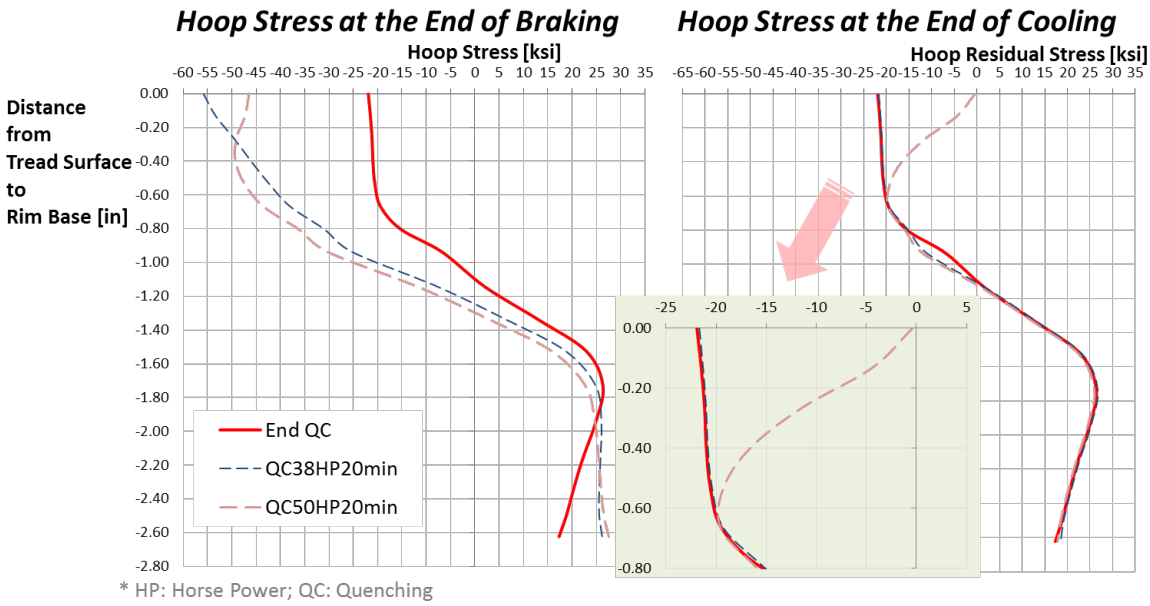

Figure 5-12. Hoop stress distribution on the cross-section of the wheel due to drag-braking: 38 HP and 50 HP for 20 minutes

The results from the stress analysis for the six stop-braking scenarios are presented in Figure 5-13, 5-14, 5-15, and 5-16. The contour plot of hoop residual stress distribution on the wheel section for stop-braking are presented in Figure 5-13. As shown in the temperature distribution, the variation of stress distribution was similar to that for drag-braking and is concentrated near the tread surface of the wheel rim. It is apparent that the descending grade and the train operating speed were important factors affecting the residual stress distribution on the wheel rim due to stop-braking.

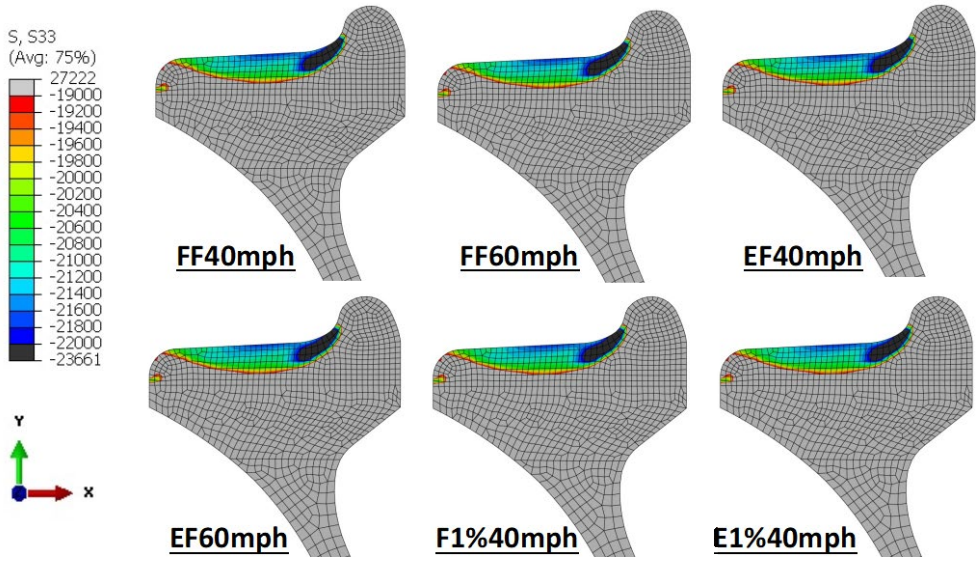

Figure 5-13. Contour plot of hoop residual stress distribution on the cross-section of the wheel due to stop-braking [psi]

The time history of hoop stress distribution on the tread surface and rim base of the wheel is presented in Figure 5-14. The maximum duration of the six stop-braking scenarios was 1 minute, 56 seconds – the normal stop condition from 40 mph (64.4 km/h) on the 1 percent descending grade track. For all scenarios, the train completely stopped within the maximum duration (1 minutes, 56 seconds). It is clear that the emergency stop cases indicated the maximum hoop stress earlier than the normal stop cases, as shown in Figure 5-14.

Figure 5-15 shows the variation of hoop residual stress distributions on the wheel section induced by the brake applications. For stop-braking conditions considered in this section, the effect on compressive hoop residual stress was similar in both normal and emergency stop conditions since neither scenario exceeded the yield stress. Figure 5-15 includes expanded view of the hoop stress distribution between the tread surface and the rim base.

As shown in Figure 5-10, Figure 5-12, and Figure 5-15, which represent the residual stress distributions for drag- and stop-braking, the depth of compressive hoop residual stress consumed below the tread surface varied for from -0.9 inch (-22.86 mm) to -0.6 inch (-15.2 mm) for drag-braking, while it remained around -0.7 inch (-17.78 mm) for stop-braking. That was due to the duration of brake loading, as was demonstrated by the different thermal loading rates in the temperature distribution on the wheel section between drag- and stop-braking.

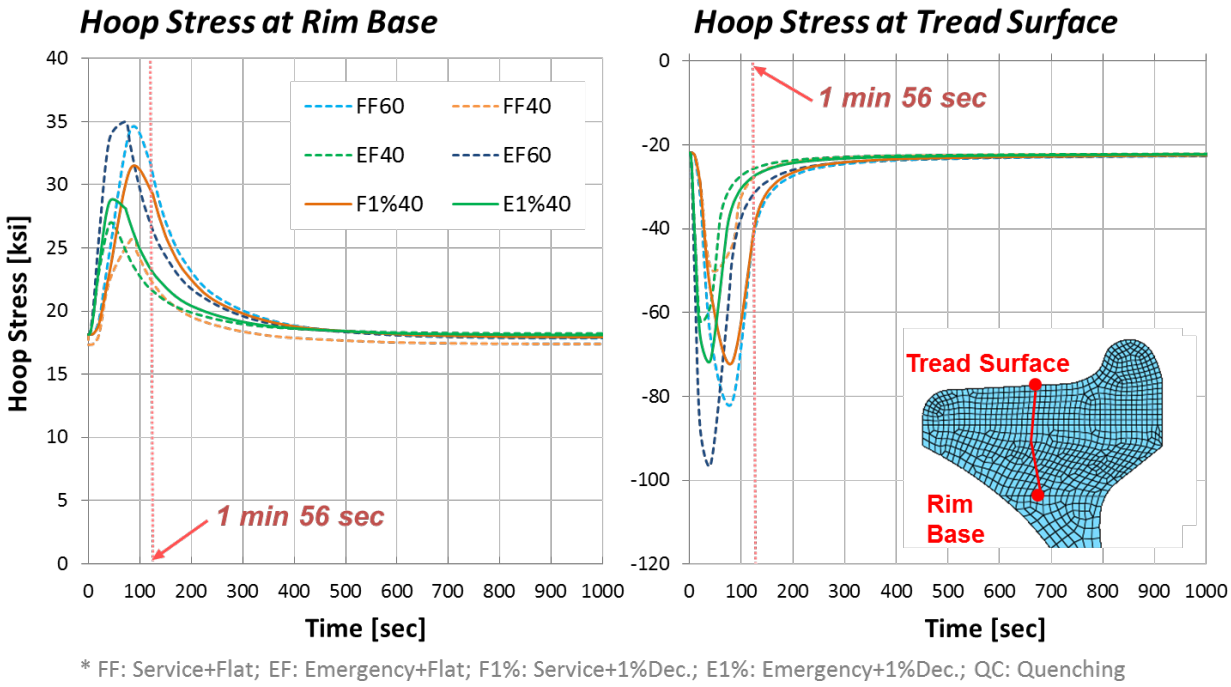

Figure 5-14. Time history of hoop stress distribution for six scenarios of stop-braking

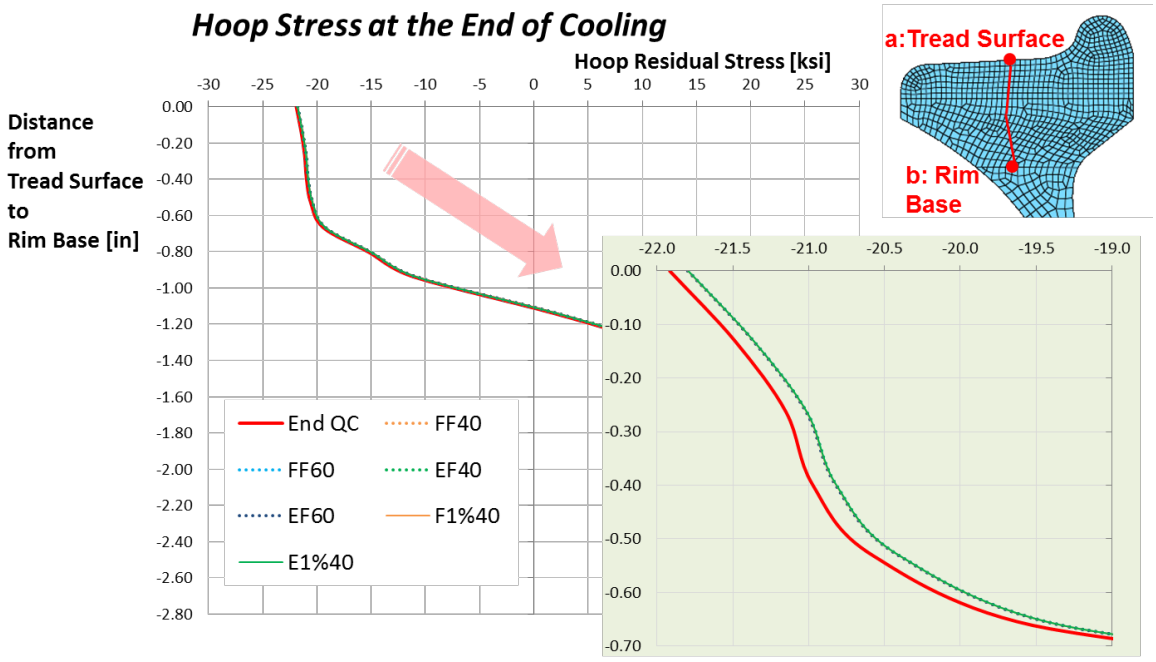

Figure 5-15. Hoop residual stress distribution on the cross-section of the wheel due to six scenarios of stop-braking: measured from base line, a-b

The results show that normal stop and emergency braking did not significantly diminish the residual hoop stress distribution introduced in the manufacturing process. Even drag-braking as prescribed for wheel design analysis in [27] did not significantly alter the residual stress distribution. However, detrimental tensile hoop residual stress could develop in the wheel rim due to severe braking conditions such as when hand brakes are left applied for extended period.

6. Modification of Residual Stress under Combined Service Condition Loads

This section focuses on estimating the state of final residual stresses in freight wheels as affected by service loads, including thermal load due to braking and traction load under curving conditions.

Analyses in this section used the same temperature-dependent material properties as for the service conditions in the previous sections. The initial residual stresses in the wheel body consisted of the stresses developed in the analysis of the heat treatment during the manufacturing process.

To determine the final residual stress distribution under service conditions, the mechanical and thermal loads were applied to the wheel after manufacturing process.

The two contact conditions selected for analysis were NT2 and NT3; the normal wheel load in the interaction of wheel and rail was 35,750 lbs (159 kN), with traction ratios of 0.29 and 0.39.

For the thermal load, two drag-braking conditions were simulated: (1) 38 HP for 20 minutes and (2) 50 HP for 20 minutes.

Figure 6-1 to 6-4 show the result of analyses in which a new wheel in the as-manufactured residual stress state was subjected to the four combinations of contact and braking loading.

As shown in Figure 6-1 and Figure 6-3, when a wheel was subjected to the normal drag-braking (38 HP for 20 minutes) as specified in AAR S-660 [27] and the mechanical loading (design load), there was small reduction, i.e., 2-3 percent, in the hoop residual stresses.

For the higher horsepower case of 50 HP, as shown in Figure 6-2 and Figure 6-4, the combined mechanical and drag-braking loading caused a drastic reduction in the hoop residual stress, almost identical to thermal load only.

The result of the combined thermal and mechanical loading condition show that the compressive stresses induced by mechanical loading tended to reduce the impact of tread-braking thermal load on residual stresses. However, under normal wheel loading, the effect is small.

The results show that with increasing braking load and duration, high temperatures caused a reduction in yield strength, and the stress on the tread surface exceeded the yield stress. For this loading, the compressive hoop residual stress on the wheel tread is significantly reduced. Such severe loading has the potential to result in tensile hoop stresses.

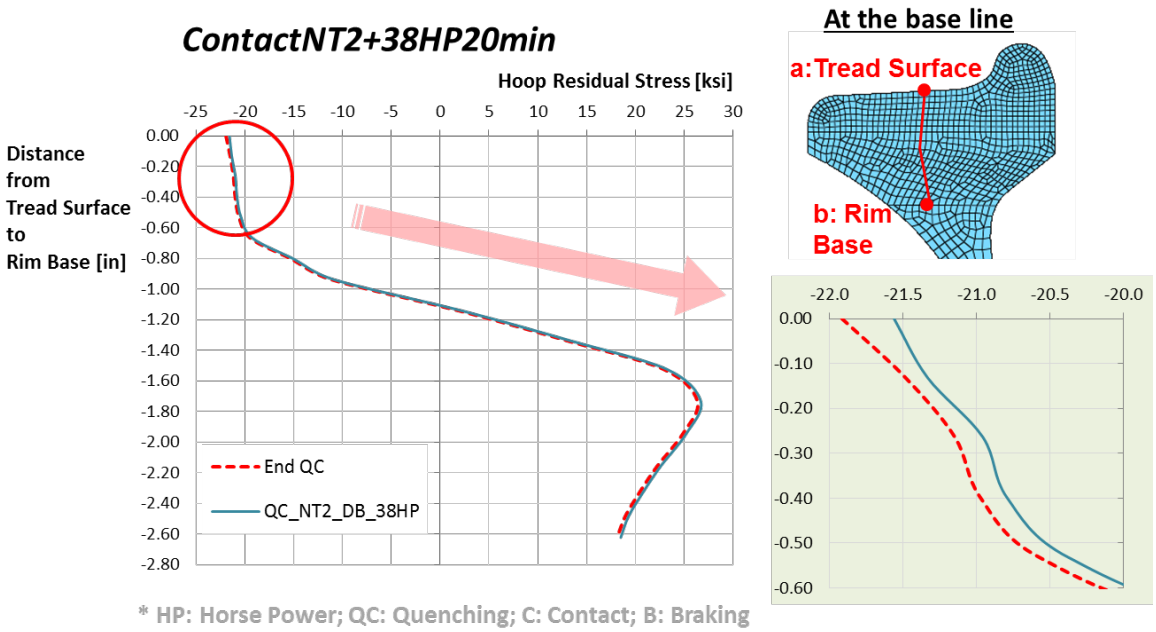

Figure 6-1. Hoop residual stress distribution on the cross-section of the wheel under the service condition: contact NT2 and 38 HP for 20 minutes

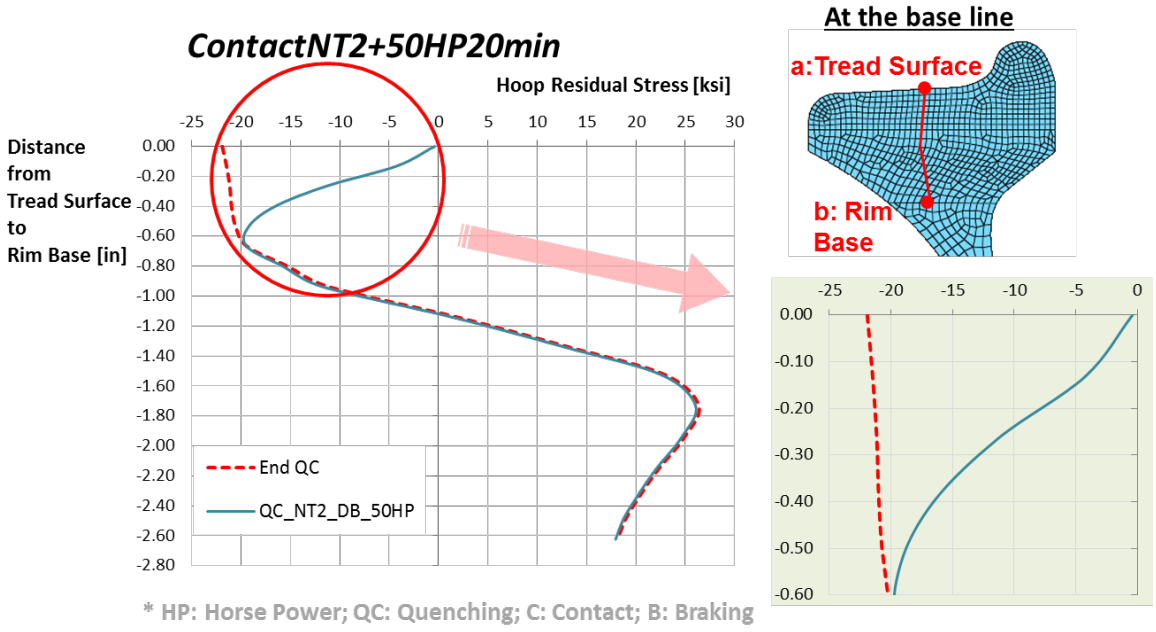

Figure 6-2. Hoop residual stress distribution on the cross-section of the wheel under the service condition: contact NT2 and 50 HP for 20 minutes

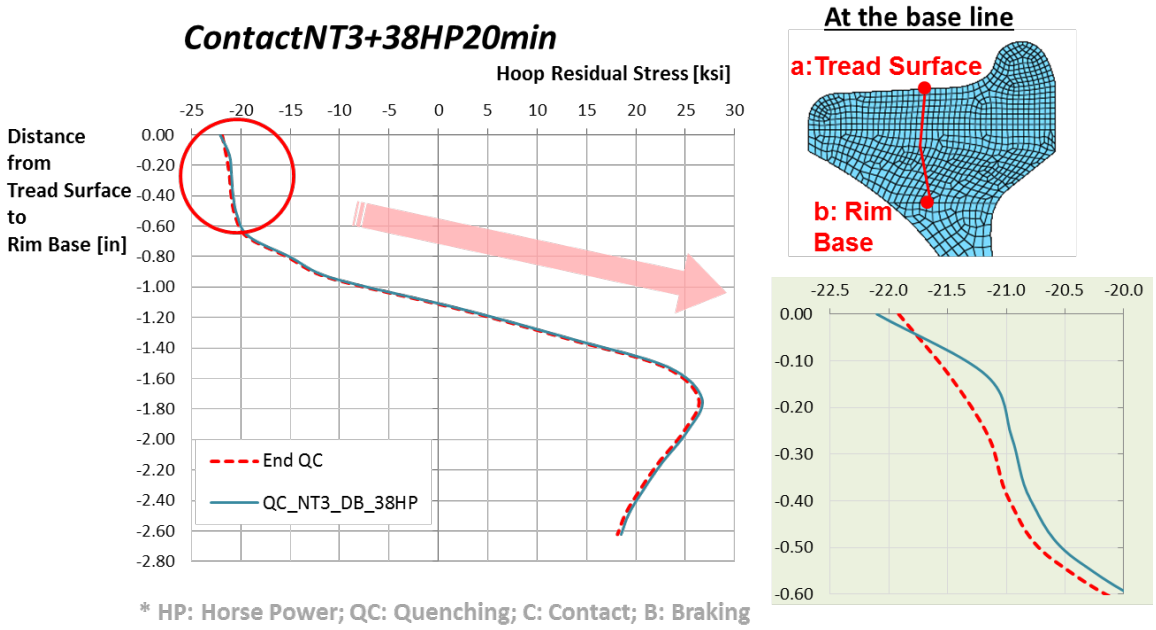

Figure 6-3. Hoop residual stress distribution on the cross-section of the wheel under the service condition: contact NT3 and 38 HP for 20 minutes

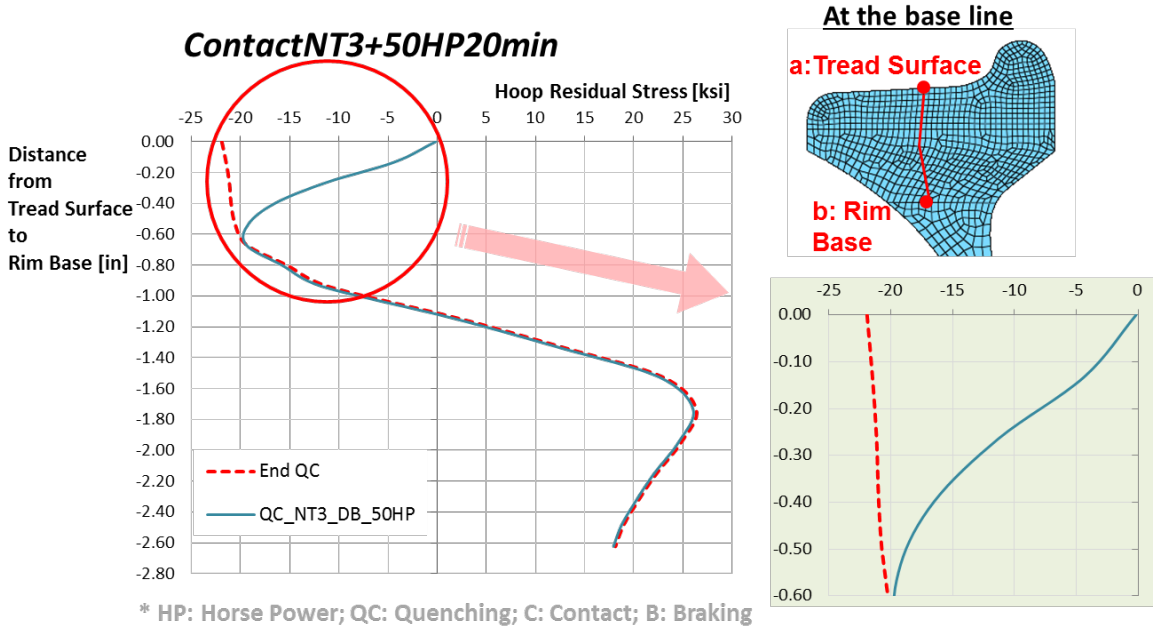

Figure 6-4. Hoop residual stress distribution on the cross-section of the wheel under the service condition: contact NT3 and 50 HP for20 minutes

7. Wheel Life Model Concept

This section describes a conceptual framework for a wheel life model. The model combines shakedown theory and the effects of residual stresses from heat treatment, mechanical contact loading, and thermal loading. The proposed approach will define the stress state of a wheel under service loads. Such knowledge can lead to an assessment and evaluation of practices that help delay crack initiation and, therefore, extend wheel life and improve safety.

7.1 Shakedown Theory

Railway vehicle weight has progressively increased over time. Although rails and wheels have been improved, the wheel-rail contact area is still subject to higher and higher stresses. These repeated high stresses have accelerated the problem of RCF. Wheels repeatedly experience rolling contact and braking loading during their service lives. These cyclic loads cause incremental fatigue damage. Shakedown theory is appropriate for estimating the effect of repeated rolling contact loads on the surface bodies in contact. Elastic or subsurface and surface plastic strains may be produced from stresses induced by rolling contact.

Shakedown is a process in which plastic deformation due to rolling contact leads to a steady state when the yield strength of the material is exceeded. The shakedown limit represents the maximum contact conditions for shakedown. For contact conditions above the shakedown limit there is continuous plastic deformation. This can lead to the formation of RCF.

The shakedown limit is plotted on a shakedown diagram in which the y-axis is the ratio of the maximum normal pressure to shear yield stress, p_0/k, and the x-axis is the ratio of tangential force to normal force, Q/P.

Figure 7-1 shows the shakedown diagram for point contacts with various shakedown limits [20, 21, 22, 23, 24]. The shakedown limits for 3D frictional rolling- and sliding-point contacts are derived from von Mises yield criteria. The shakedown limits may vary depending on the ratio of semi-axes of contact ellipse (a/b) such as the example for a/b of 1.6, as shown in Figure 7-1. Figure 7-2 shows the elastic and elastic shakedown limits selected in this study.

RCF failures of railway wheels are divided into surface- or subsurface-initiated. For pure normal stress, first yield occurs at a point below the surface, since the state of stress at the surface nearly contains uniaxial stresses. The surface stresses increase under tangential traction. When the traction coefficient is above 0.25, as shown in Figure 7-2, first yield occurs at the surface. Thus, the normalized load with the higher traction coefficient lies above the shakedown limit, the repeated plastic deformation takes place, and the material at the surface is deformed.

In some cases, wear is dominant in the wheel life since wheel wear reduces the rim thickness and changes the tread profile due to the surface material removal under service conditions. Thus, the normalized load located far away from shakedown limits may induce wear instead of rolling contact damage.

The residual stress distribution due to the manufacturing process does not represent a shakedown state since it occurs only once.

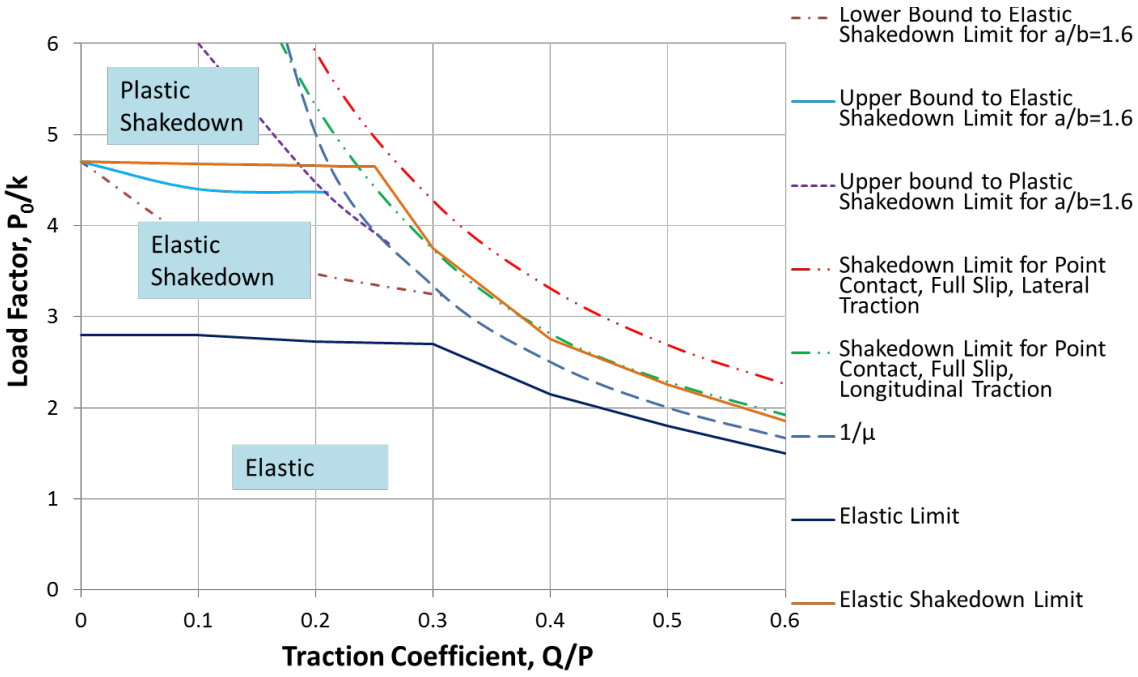

Figure 7-1. Shakedown diagram for point contacts [20, 21, 22, 23, 24]

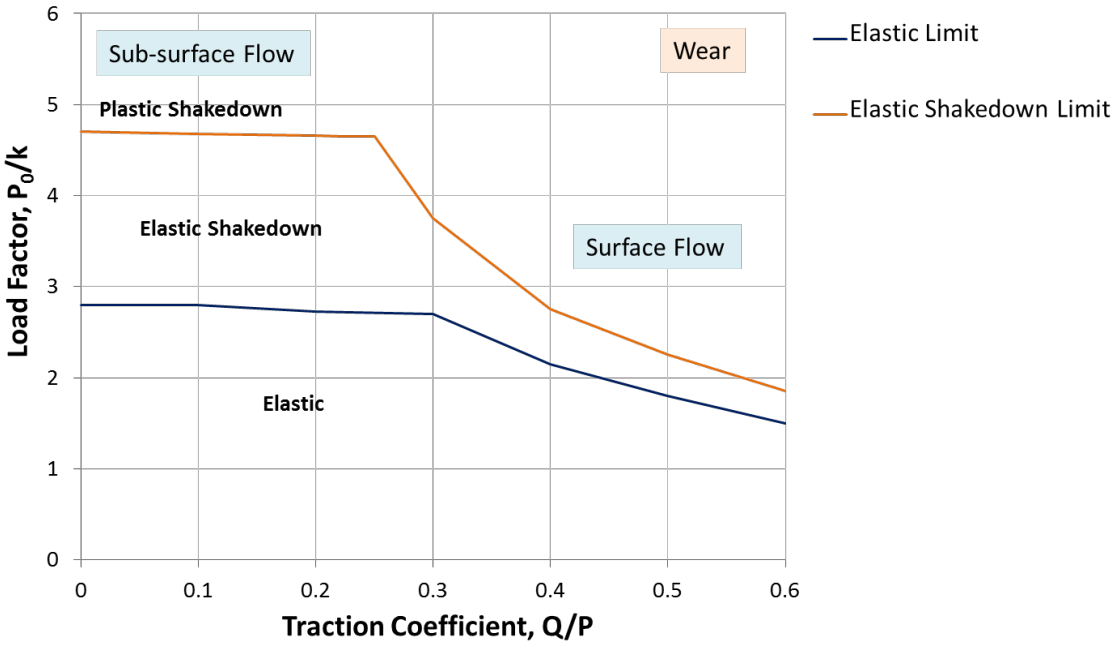

Figure 7-2. Shakedown diagram selected for determining crack initiation from RCF

7.2 RCF Crack Initiation Model

7.2.1 Shakedown Map

This study proposes a RCF crack initiation model similar to the classic shakedown map. In general, analyses using the shakedown map consider the yield stress in shear at room temperature. However, material strength varies with the temperature. Under high temperature condition and reduced yield threshold, thermal stresses can contribute to plastic flow and lead to failure in rolling contact.

Figure 7-3 shows the temperature-dependent material properties of wheel steel for tensile and shear yield stresses and the modulus of elasticity used in the analysis. The slope of the curves dramatically decreases when the wheel temperature is above 750 °F (399 °C). Such a temperature can be induced by the thermal load due to severe braking conditions.

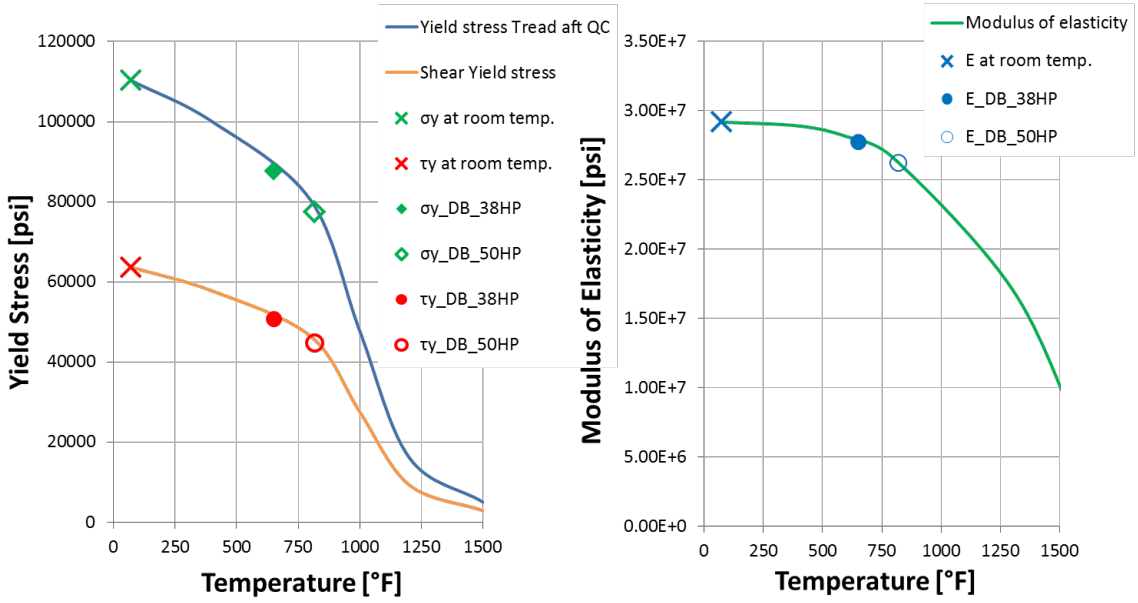

* DB: Drag Braking; SB: Stop Braking; HP: Horse Power; F1%: Service+1%Dec.; QC: Quenching

(a) (b)

Figure 7-3. Temperature dependent material properties: (a) tensile and shear yield stresses and (b) modulus of elasticity

The reduction in shear yield stress at elevated wheel temperature under braking conditions cannot be ignored. Figure 7-4 shows the result of various wheel load conditions under mechanical and thermal loads. When only the mechanical loads were considered (contact NT1, NT2, and NT3), those conditions were positioned below the elastic shakedown limit except for the case with the highest traction coefficient (contact NT3). On the other hand, when the mechanical and thermal loads were both considered, the material strength decreased due to increasing wheel temperature during tread-braking, and then the normalized load for those cases were mostly positioned above the elastic shakedown limit in which RCF may have occurred on the tread surface.

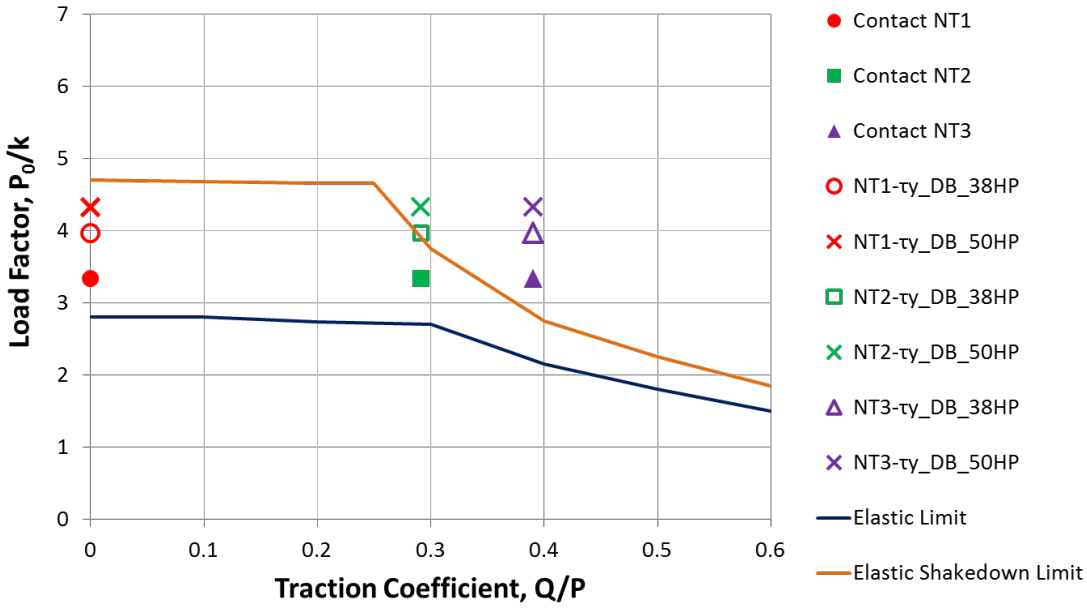

Figure 7-4. Shakedown results with consideration for updated material properties

7.2.2 Proposed Model

The RCF crack initiation model suggested in this study was used to determine the beginning of RCF under or on the surface of wheel treads. The conventional shakedown limit does not reflect the residual stress distribution from the manufacturing process. To address the issue, a parametric model of RCF crack initiation as a generic function of wheel load, material strength, traction coefficient, and hoop residual stress on the wheel tread surface is proposed as follows:

$$d_{RCF\_CI} = f(p_o, k, \mu, \sigma_{hres}) \tag{7.1}$$

Where,

d_{RCF_CI}	is the RCF crack initiation index,
p_o	is the maximum normal pressure,
k	is the shear yield stress,
μ	is the traction coefficient, and
σ_{hres}	is the hoop residual stress.

The RCF crack initiation model has four different levels of damage, as follows:

- *Region I:* No RCF initiated with compressive hoop residual stress.
- *Region II:* No RCF initiated with tensile hoop residual stress.
- *Region III:* RCF initiated with compressive hoop residual stress.
- *Region IV:* RCF initiated with tensile hoop residual stress.

Table 7-1 shows the conditions that determine which type of RCF damage the wheel would experience. The potential RCF damage on the tread surface and subsurface increases from Region I to Region IV. The criterion for the proposed model is schematized in Figure 7-5. This diagram was developed from the shakedown diagram by adding an axis representing the hoop residual stress. The model approach is based on the correlation between residual stress and RCF initiation. According to the state of residual stress and load factor, each region in the model considers whether an RCF crack has been initiated.

Table 7-1. Definition of RCF crack initiation model

	Subsurface ($\mu < 0.25$)		Surface ($\mu > 0.25$)	
	σ_{hres}	p_o/k	σ_{hres}	p_o/k
Region I	< 0	$< ESL_{subsf}$	< 0	$< ESL_{sf}$
Region II	> 0	$< ESL_{subsf}$	> 0	$< ESL_{sf}$
Region III	< 0	$> ESL_{subsf}$	< 0	$> ESL_{sf}$
Region IV	> 0	$> ESL_{subsf}$	> 0	$> ESL_{sf}$

σ_{hres} = Hoop residual stress
μ = Traction coefficient
p_o/k = Ratio of normal pressure to shear yield stress
$ESL_{subsf\ or\ sf}$ = Elastic shakedown limit for subsurface or surface

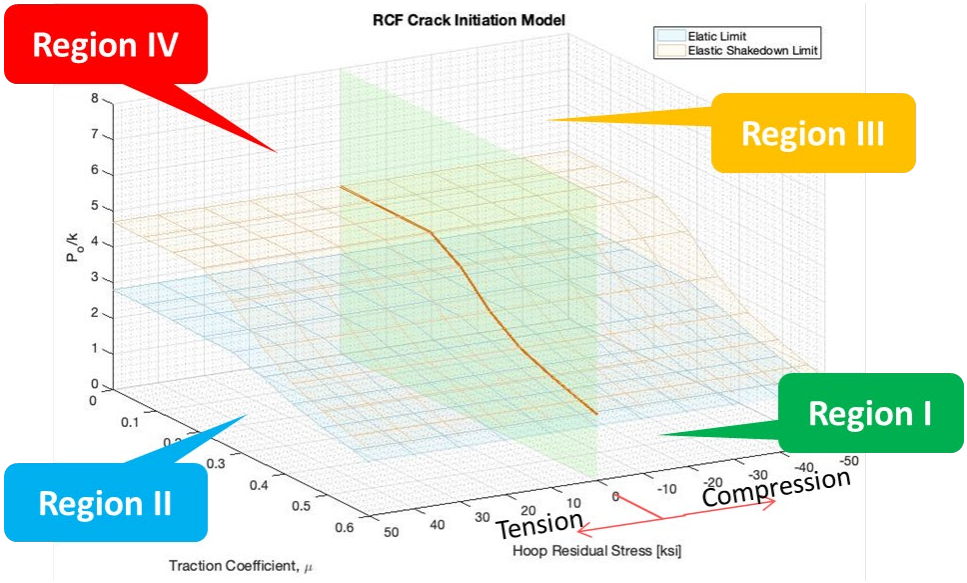

Figure 7-5. Concept of RCF crack initiation model

A flowchart for the wheel damage model is shown in Figure 7-6. The proposed model included the following conditions:

1. Residual stresses due to heat treatment
2. Mechanical loads (vertical, lateral, and longitudinal forces) for 36-ton axle load service
3. CONTACT models for three different friction coefficients
4. Material properties for AAR Class C steel
5. Braking thermal loads

According to the procedure in Figure 7-6, the parameters, such as residual stress due to the manufacturing process, rolling contact mechanical loads, thermal loads due to tread-braking, and temperature-dependent material properties under various thermal loads, are required in the model to determine the wheel's state of damage.

As an example, the results reported in the previous sections were used for the required parameters in the wheel damage model. Figure 7-7 and Table 7-2 show the RCF crack initiation state for the combinations of mechanical and thermal loads.

Contact NT1 and NT2 cases only considered the mechanical load. Those cases were within Region I, since RCF was not initiated and there was compressive hoop residual stress on the wheel tread.

The other cases that include contact NT3 and four cases with the combination of mechanical and thermal loads were in Region III, since RCF occurred with the compressive hoop residual stress on the wheel tread. Thus, it was expected that the compressive hoop residual stress helped to prevent or delay crack opening on the surface of wheel tread.

Even though these cases were within Region III, for two cases of 50 HP drag-braking among the four cases, note that their index may change from Region III to Region IV. The reason is that the RCF crack initiation index for those two cases was very close to the boundary between Region III and Region IV, since the compressive hoop residual stress was nearly consumed.

As shown in the result of example cases, two other cases with the severe drag-braking of the long duration or higher horsepower were within Region IV. Under such a state, a crack may propagate on the tread surface of a wheel due to the reversal of hoop residual stress from compressive to tensile if the wheel is subjected to additional mechanical and thermal loads.

The wheel damage model with RCF crack initiation proposed in this study cannot quantitatively estimate the fatigue life of the wheel, but it does provide the state of wheel condition with consideration for RCF crack initiation. Its results could be used to determine wheel fatigue life by modeling crack propagation and accumulation of damage under varying thermal and mechanical loading conditions in revenue service.

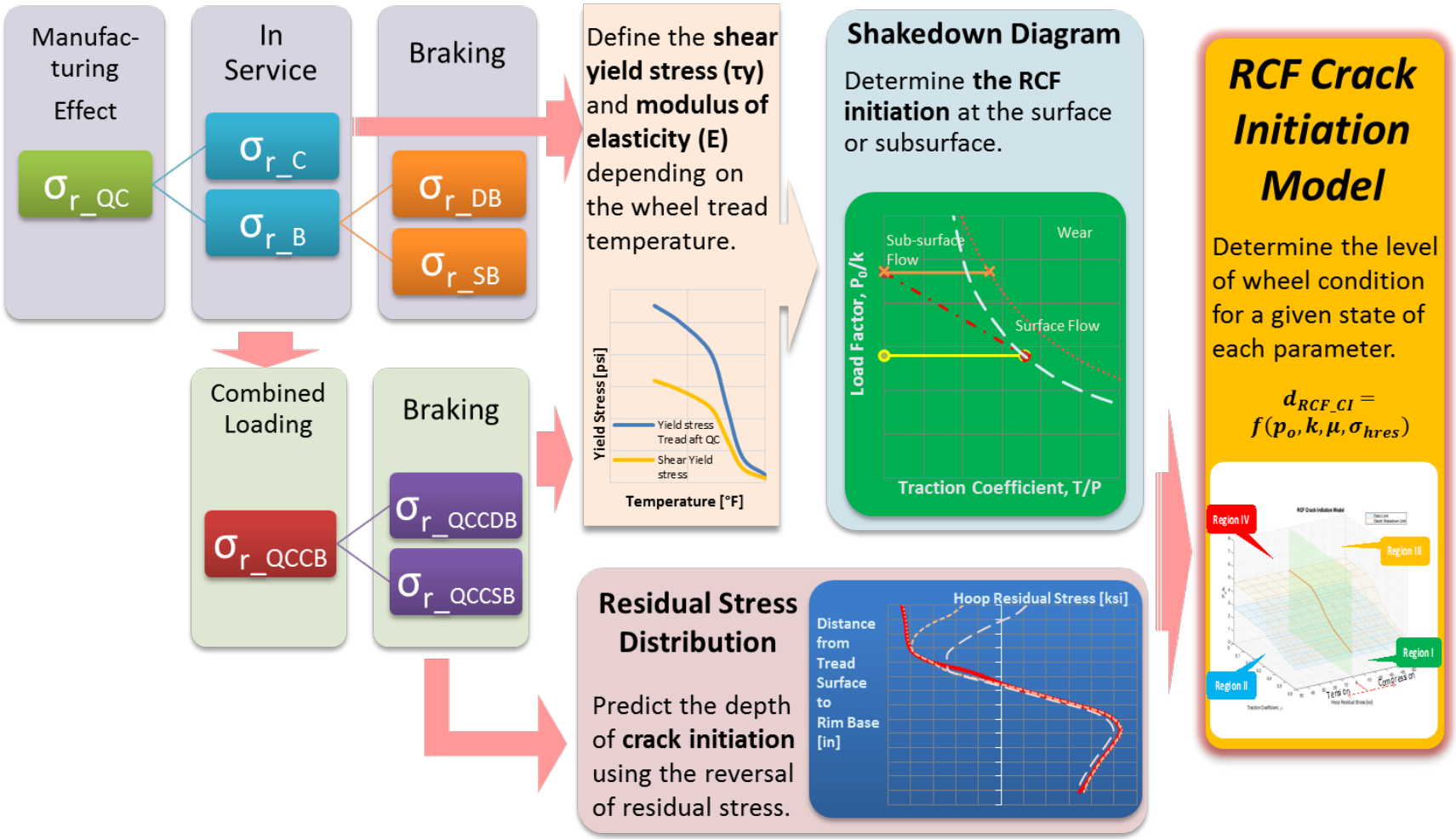

Figure 7-6. Flowchart of framework for determining crack initiation by RCF

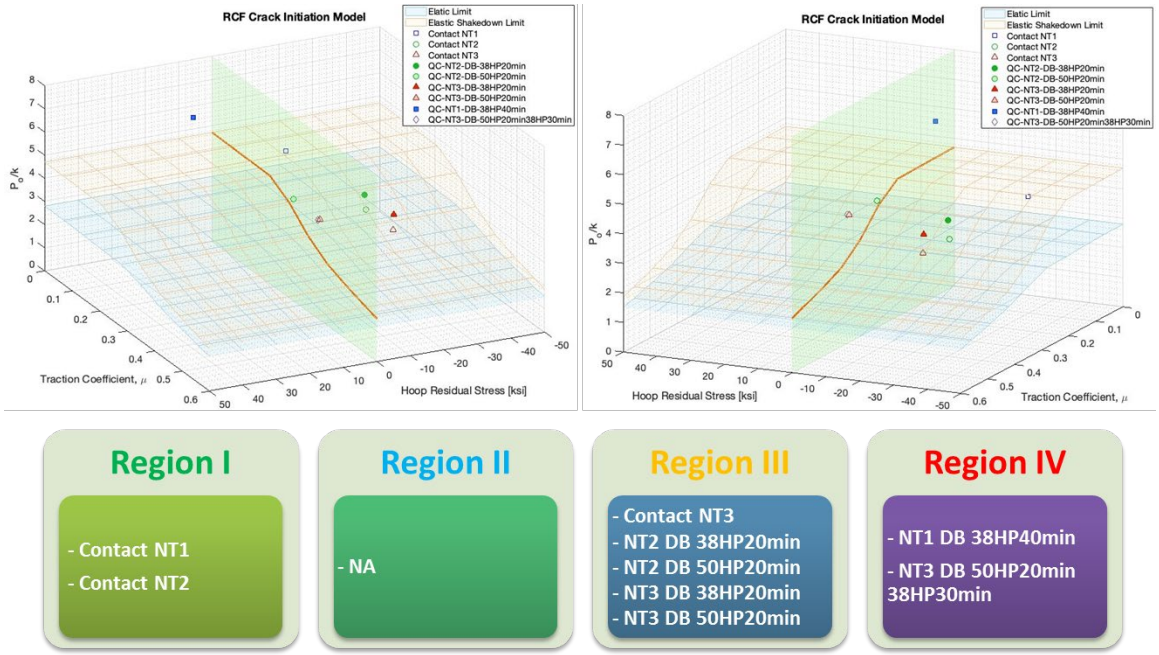

Figure 7-7. Visual expression of determining RCF crack initiation for example cases

Table 7-2. RCF crack initiation results for example cases

Case	μ	p_o/k	σ_{hres} [ksi]	*Region*
Contact NT1	0.00	-21.92	3.33	Region I
Contact NT2	0.29	-21.92	3.33	Region I
Contact NT3	0.39	-21.92	3.33	Region III
NT1 DB 38HP40min	0.00	5.67	5.50	Region IV
NT2 DB 38HP20min	0.29	-21.56	3.97	Region III
NT2 DB 50HP20min	0.29	-0.39	4.33	Region III
NT3 DB 38HP20min	0.39	-22.10	3.97	Region III
NT3 DB 50HP20min	0.39	-0.18	4.33	Region III
NT3 DB 50HP20min 38HP30min	0.39	0.56	4.33	Region IV

8. Conclusion

This report described the result of Phase I efforts toward developing a wheel life model. It included gathering and reviewing the literature to understand mechanisms and analytical methods of how the life of wheel is affected by the material properties, manufacturing process, and mechanical and thermal loads in service.

An AAR Class C 36-inch wheel with one-wear was selected for the analysis. The nonlinear FEA study focused on estimating the magnitude and trend of hoop residual stress distribution in the wheel rim due to the manufacturing process. During the heat treatment process, the material properties of wheel changed depending on the transformed microstructure in the wheel; residual stresses were also developed in the wheel. The compressive hoop residual stress in the wheel rim helped delay contact fatigue and crack initiation on the tread surface and subsurface, respectively.

The analysis was extended to determine the effect of service, mechanical, and thermal loads on the residual stress state in the wheel rim. For the contact loads, the residual stress distribution modified due to the effect of contact stresses was confined to a region very near the wheel tread surface, depending on traction coefficient. As the traction coefficient increased, the compressive residual stress also tended to increase at the tread surface and the subsurface immediately below.

Whereas tread-braking under drag- and stop-braking produced significant thermal stresses in the tread and rim areas, the stresses did not generally diminish the residual stresses created by the manufacturing process. However, wheels may occasionally experience severe thermal loading, which can diminish the beneficial hoop residual stress in the tread and rim significantly – and even result in tensile stresses, depending upon the duration and severity of the braking load.

For combined loading under service conditions, even with the beneficial compressive stresses induced by mechanical loading, stress reversal may occur in the tread portion of the wheel due to severe thermal loading, heavy braking, and longer duration. It could lead to the shortening of the crack initiation period and the propagation life.

Based on the analyses, a parametric model derived from shakedown theory was proposed as a function of wheel load, material strength, traction coefficient, and hoop residual stress on the wheel tread. The RCF crack initiation model proposed in this study was not predictive of the fatigue life of the wheel, but it would provide the state of wheel conditions with consideration for RCF crack initiation. Furthermore, the model can be used to assess and change the operating environment to improve the wheel fatigue life.

Phase II will focus on developing the model to simulate crack propagation by including phenomena, such as modeling fluid entrapment and metallurgical defects. Phase II aims to simulate crack propagation life under developed wheel operation scenarios as well as the approach to include wear and its effect on the fatigue performance of wheel treads and rims.

9. References

1. Federal Railroad Administration. (2020). FRA safety database. Retrieved from http://safetydata.fra.dot.gov/
2. Tournay, H., & Cakdi, S. (2016). Performance evaluation of improved freight bogie suspension systems. The 11th World Congress on Railway Research, Italy.
3. Leeper, J., & Allen, R. (2015). *Guidelines to Best Practices for Heavy Haul Railway Operations: Management of the Wheel and Rail Interface*. Virginia Beach, Virginia: International Heavy Haul Association.
4. Cakdi, S., Cummings, S., & Punwani, J. (2015). Heavy haul coal wagon wheel load environment – rolling contact fatigue investigation. Joint Rail Conference, San Jose, CA.
5. Association of American Railroads. (2015). Field manual of the AAR interchange rules. RULE 41. Why Made Code, 351-352
6. Kulhman, C., Sehitoglu, H., & Gallagher, M. (1988). The significance of material properties on stresses developed during quenching of railroad wheels. *Proceedings of the 1988 Joint ASME IEEE Railroad Conference*, 55-63.
7. Gordon, J., & Perlman, A. B. (2003). Estimation of residual stresses in railroad car following manufacture (DOT/FRA/ORD-03/24). Washington, DC: U.S. Department of Transportation, Federal Railroad Administration.
8. Wang, K., & Pilon, R. (2002). Investigation of heat treating of railroad wheels and its effect on braking using Finite Element Analysis. *Proceedings of the 10th International ANSYS Conference and Exposition*, Pittsburgh.
9. Gordon, J., Jones, J.A., & Perlman, A. B. (1998). Evaluation of service-induced residual stresses in railroad commuter car wheels. *Proceedings of the International Mechanical Engineering Congress and Exhibition*, Anaheim, CA. ASME RTD 15.
10. Kalker, J.J. (1991). Wheel-rail rolling contact theory. *Wear*, 144 (1-2) 243-261.
11. Johnson, K.L. (1985). *Contact Mechanics*. Cambridge, U.K.: Cambridge University Press.
12. Vollebregt, E.A.H., & Kalker, J. J. (2019). CONTACT (Version 19.1). VORtech.
13. Vollebregt, E.A.H. (2019). User guide for CONTACT, Rolling and sliding contact with friction (Technical Report TR09-03, Version 19.1). VORtech. www.cmcc.nl.
14. Kalker, J.J. (1982). A fast algorithm for the simplified theory of rolling contact. *Vehicle System Dynamics,* 11, 1-13.
15. Vollebregt. E.A.H., & Wilders, P. (2011). FASTSIM2: A second-order accurate frictional rolling contact algorithm. *Computational Mechanics,* 47:105–116, DOI 10.1007/s00466-010-0536-7.
16. Lundén, R. (1991). Contact region fatigue of railway wheels under combined mechanical rolling pressure and thermal brake loading. *Wear,* 144, 57-70.

17. Kabo, E., & Ekberg, A. (2002). Fatigue initiation in railway wheels-on the influence of defects. *Wear*, 253, 26-34.

18. Ekberg, A., & Kabo, E. (2005). Fatigue of railway wheels and rails under rolling contact and thermal loading – an overview. *Wear*, 258, 1288-1300.

19. Magel, E.E. (2011). Rolling contact Fatigue: A comprehensive review (DOT/FRA/ORD-11/24). Washington, DC: U.S. Department of Transportation, Federal Railroad Administration.

20. Johnson, K.L. (1989). The strength of surfaces in rolling contact. *Proceedings of the Institution of Mechanical Engineers, Part C: Mechanical Engineering Science*, 203 (3) 151-163.

21. Ponter, R.S., Hearle, A.D., & Johnson, K.L. (1985). Application of the kinematical shakedown theorem to rolling and sliding point contacts. *Journal of the Mechanics and Physics of Solids*, 33 (4) 339-362.

22. Bower, A.F., & Johnson, K.L. (1991). Plastic flow and shakedown of the rail surface in repeated wheel-rail contact. *Wear*, 144, 1-18.

23. Bower, A.F., & Johnson, K.L. (1993). Shakedown, residual stress and plastic flow in repeated wheel-rail contact. *Rail Quality and Maintenance for Modern Railway Operation*, 239-249.

24. Johnson, K.L. (1990). A graphical approach to shakedown in rolling contact. *Applied Stress Analysis*, 263-274.

25. Ericsson, T. (1991). Principles of heat treating of steels. *Heat Treating*, Vol 4, ASM Handbook, ASM International.

26. Gordon, J. (1998). Estimation of residual stresses in railroad car wheels resulting from manufacture and service loading. MS Thesis, Department of Mechanical Engineering, Tufts University.

27. Association of American Railroads. (2015). Manual of standards and recommend practices, Section G, Wheels and Axles.

28. Dossett, J. L., & Boyer, H. E. (2006). *Practical Heat Treating* (2nd ed.). ASM International, Materials Park, Ohio.

29. Dassault Systemes. (2014). ABAQUS (Version 6.14-2). Dassault Systèmes Simulia Corp.

30. Dassault Systemes. (2014). ABAQUS/CAE User's guide (Version 6.14). Dassault Systèmes Simulia Corp.

31. Milošević, M., Miltenović, A., Banić, M., & Tomić, M. (2017). Determination of residual stress in the rail wheel during quenching process by fem simulation. *Facta Univesitatis Series Mechanical Engineering*, 15 (3) 413-425.

32. Totten, G. E. (2007). *Steel Heat Treatment: Metallurgy and Technologies*. Boca Raton, FL: CRC Press.

33. Liščić, B., Tensi, H. M., & Luty, W. (1992). *Theory and Technology of Quenching*. Berlin: Springer-Verlag.

34. Tang, Y.H., Gordon, J.E., Perlman, A.B., & Orringer. O. (1993). Finite element models, validation, and results for wheel temperature and elastic thermal stress distributions (DOT/FRA/ORD-93/17). Washington, DC: U.S. Department of Transportation, Federal Railroad Administration.
35. Cummings, S. M., & Lauro, D. (2008). Inspections of tread damaged wheelsets. *Proceedings of ASME Rail Transportation Division Fall Technical Conference*, Chicago.
36. MathWorks. (2019). MATLAB (Version R2019a). The MathWorks, Inc.
37. DeltaRail. (2016). VAMPIRE Pro (Version 6.40). DeltaRail Group Limited.
38. Federal Railroad Administration. (2015). Validation of the Train Energy and Dynamics Simulator (TEDS) (DOT/FRA/ORD-15/01). Washington, DC: U.S. Department of Transportation.

Abbreviations and Acronyms

AAR	Association of American Railroads
ESL	Elastic Shakedown Limit
FASTSim	Future Automotive Systems Technology Simulator
FE	Finite Element
FEA	Finite Element Analysis
FRA	Federal Railroad Administration
GRL	Gross Rail Load
HP	Horsepower
HTA	Heat Transfer Analysis
HTC	Heat Transfer Coefficient
RCF	Rolling Contact Fatigue
SA	Stress Analysis
TEDS	Train Energy and Dynamics Simulator
TTT	Time-Temperature-Transformation